Geology, geochemistry and sulphur isotopes of the Hat Han gold–antimony deposit, NE Vietnam

Trong Hoa Tran [a,*], P.A. Nevolko [b,c], Thi Phuong Ngo [a], T.V. Svetlitskaya [b], Hoang Ly Vu [a], Yu.O. Redin [b,c], Tuan Anh Tran [a], Thi Dung Pham [a], Thi Huong Ngo [a]

[a] *Institute of Geological Sciences, Vietnam Academy of Science and Technology, 84 Chua Lang, Dong Da, Hanoi, Viet Nam*
[b] *Institute of Geology and Mineralogy, Siberian Branch of the Russian Academy of Sciences, 3 Koptyug ave., 630090 Novosibirsk, Russia*
[c] *Novosibirsk State University, 2 Pirogova str., 630090 Novosibirsk, Russia*

ABSTRACT

The Song Hien Rift basin is considered as one of the important regions for gold deposits in North East Vietnam. Host rocks of a number gold deposits in the Song Hien Rift basin are mainly in Lower Triassic sedimentary formations. However, there is the Hat Han gold deposit hosted in fined-grained mafic magmatic rocks with similar characteristics as gold deposit hosted in the Triassic sediments. Sulphur isotopic compositions of sulphide are similar to those in carbonaceous shale, suggesting that the sulphur was 'borrowed' from sedimentary rocks in filling the rift basin. Gold-bearing sulphides (pyrite and arsenopyrite) are the main form of Au presence in the ore. Gold in pyrite is present as Au^{+1}, and a minor amount of as nanoparticles of native Au (Au^0); whereas in arseno-pyrite, gold is chemically bound as the octahedral complex $AuAs_2$. Analysis of geology, as well as geochemical and isotopic studies show that the genesis of the Hat Han gold deposit is not related to the Cao Bang mafic magmatism; instead the latter only serves as (ore) host rock. The geochemical results presented above suggest that the gabbro host rock only supplies iron needed for sulphide formation. With regard to ore genesis, the Hat Han gold deposit in the Song Hien rift basin was generated in the similar way as sediment-hosted gold deposit. There are many similar typomorphic features between the Hat Han deposit and Carlin-like deposits in the Nanpanjang sedimentary basin in China.

© 2016 Elsevier B.V. All rights reserved.

1. Introduction

The geology of Northern Vietnam was studied only from the second half of the 20th century by a group of Russian and Vietnamese geologists whereas establishing a geological map at 1:500,000 (Dovzhikov et al., 1965). Since then a number of works on regional geodynamics and magmatic events have been carried out (Faure et al., 2014; Hoa et al., 2008; Leloup et al., 1995; Lepvrier et al., 1997, 2008, 2011; Liu et al., 2012; Tapponnier et al., 1990; Zhang et al., 2013); however, studies of mineral systems in Northern Vietnam are rare.

One of the areas considered important for metallogenic studies is the Song Hien Rift basin in Northeastern Vietnam. The basin consists mainly of Triassic sulphide-rich black shale beds, which play a role in sediment-hosted formation for various mineral systems such as antimony, mercury and gold-sulphide deposits (Hoa et al., 2008).

The Triassic Song Hien sedimentary basin, trending NW–SE along the Sino-Vietnam boundary, is an intra-continental rift, whose formation may be associated with the Emeishan mantle plume (Hoa et al., 2008; Izokh et al., 2005; Polyakov et al., 2009; Vladimirov et al., 2012).

To the northwest, in Guangxi and Yunnan provinces of China, analogous sedimentary basin to the Song Hien is Nanpanjang (Youjiang Basin) (Galfetti et al., 2008; Guangxi BGMR, 1985). Hosting a number of gold deposits, Nanpanjang is included in a regional metallogenic region termed as "golden triangle" (Chen et al., 2011; Peters et al., 2007; Zhong et al., 2002; Zhou et al., 2002).

Host rocks of a number gold deposits in the "golden triangle" are mostly Mesozoic (and rarer Paleozoic) argillite, sandstone, and small amount of limestone and volcaniclastics (Peters et al., 2007). Similar lithologies are also observed in the Song Hien Rift basin in northeastern Vietnam, where gold deposits are hosted mainly in Lower Triassic formations.

However, there is the Hat Han gold deposit hosted in fined-grained mafic magmatic rocks with similar characteristics as gold deposit hosted in the Triassic sediments. In the "golden triangle" of Yunnan, China, host rocks of the Jimba gold deposit are argillaceous siltstone, tuffaceous rock, gabbro, and diabase sills (Peters et al., 2007). The Anna gold deposit occurs within gabbro and diabase intrusions in Funing county, Yunan province, China. Mineralisation in the deposit consists of barren milky quartz veins or veinlets, disseminated gold-bearing arsenian pyrite and arsenopyrite within altered diabase (Dong et al., 2014). The Badu gold deposit, located in the southwest of Tianlin

* Corresponding author.
E-mail address: tronghoa-tran@igsvn.ac.vn (T.H. Tran).

county, Guangxi province, is a gold deposit occurred in diabase (Li et al., 2014). Similar instance in the Song Hien basin is the Hat Han mineralised spot located on the boundary between Ha Giang and Cao Bang provinces in the Northeastern Vietnam (Fig. 1). The mineralisation is hosted in gabbro-dolerite-diabase magmatic association of the Cao Bang complex ($\nu T1cb$) (Hoa et al., 2008).

In this study, we report on the petrography of ore-host gabbroids, ore-mineral compositions, geochemical characteristics and sulphur isotopic compositions of the sulphide minerals, and metasomatic activities having occurred during the ore-genesis. Using information of gold deposit hosted in gabbroids we will compare with those in sediment hosted.

2. Geology

2.1. Regional geological setting

Northeast Vietnam is a part of the North Vietnam–South China continental block, and comprises several regional tectonic units, such as the Song Chay Dome, the Lo Gam and Phu Ngu Palaeozoic fold belts, and the Song Hien–An Chau Late Permian–Mesozoic intra-continental rift system (Fig. 1A).

The Song Hien structure in northeast Vietnam is a rift-like (rift-genetic) volcano-terrigenous depression (Hoa et al., 2008; Tri and Vu, 2011), which is bounded be the Cao Bang–Tien and Yen Minh–Ngan Son regional fault systems to the NE and SW, respectively, and extends for >200 km in a NW–SE direction from the Vietnam–China border. In China's territory, the Nanpanjang rift-genetic basin is considered to be a continuation of the Song Hien structure (Galfetti et al., 2008; Guangxi BGMR, 1985).

The basin fill of the Song Hien depression comprises mainly Devonian and Triassic terrigenous sediments (Fig. 1B), and minor Carboniferous–Permian limestones. The Devonian formations consist of shale (and black shale), siltstone, and sandstone with minor limestone. The Early Triassic Song Hien Formation is composed of terrigenous sediments, with thick effusive members in the lower part of the stratigraphic sequence (Tri and Vu, 2011). This formation is characterised by
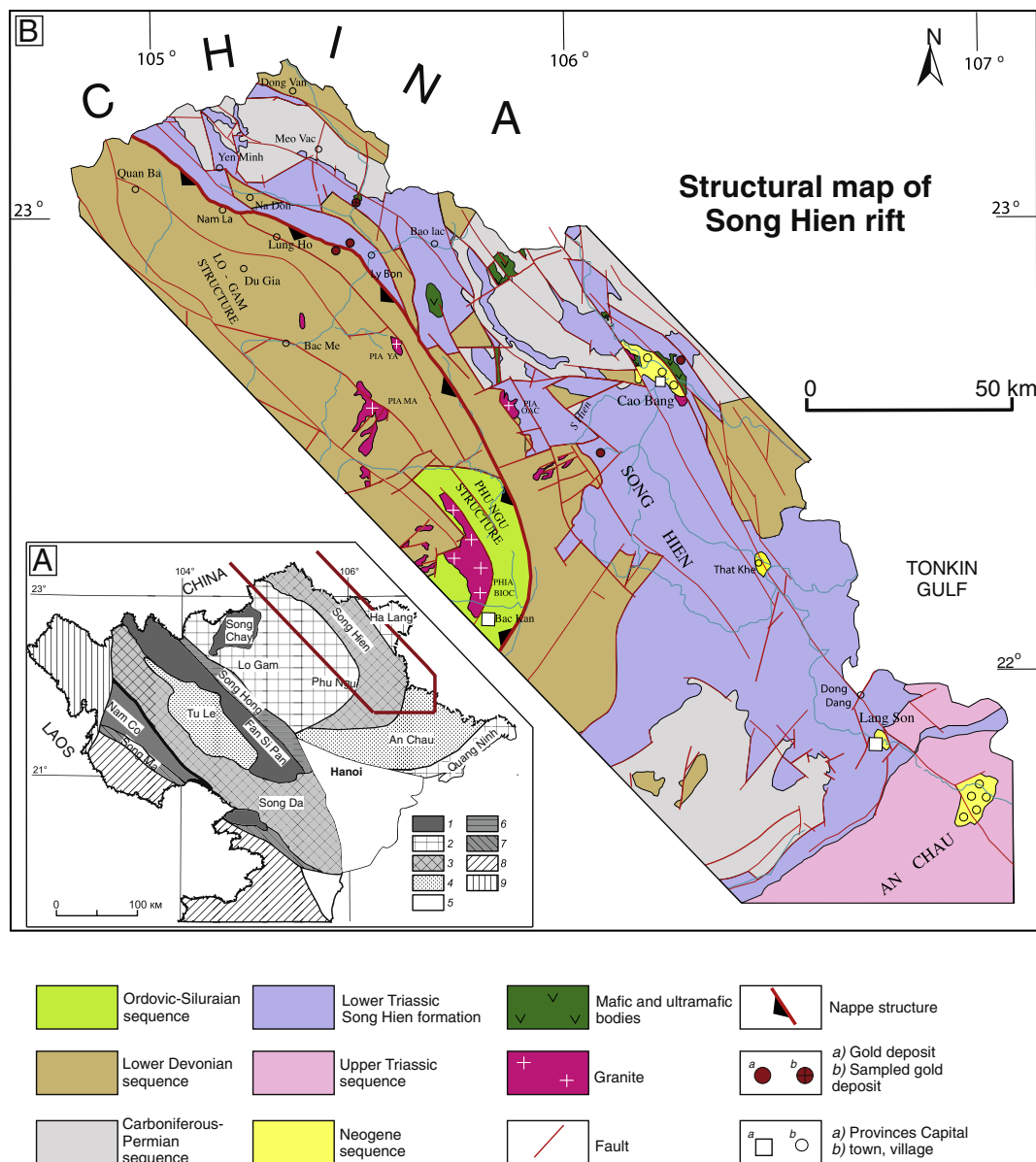
Fig. 1. (A) Simplified tectonic scheme of Northern Vietnam: 1 — Proterozoic basement; structural-formational complexes: 2 — Early-Middle Paleozoic, 3 — Permo-Triassic, 4 — Jurassic–Cretaceous; 5 — Quaternary deposits; 6 — Song Hong shear zone; 7 — Song Ma suture; 8 — Indosinian terranes; 9 — Sibumasu terrane (Hoa et al., 2008). (B) Regional structural map of the Song Hien rift showing the location of the sampled gold deposit (modified from Lepvrier et al., 2011).

widespread distribution of gravelstone, tuffaceous gritstone shale, organic- and sulphide-rich black (coal-bearing) shale, and greyish fine sandstone. The Devonian and Triassic sediments were intensively deformed, folded, and fractured during tectonic activity. Within the Song Hien basin, bounded by the above-mentioned Cao Bang–Tien Yen and Yen Minh–Phu Luong regional NW–SE faults, local NE–SW faults are widely developed.

Permian–Triassic basalt–rhyolite associations are also widespread within the basin. Other igneous rocks include gabbro-dolerite, gabbronorite and lherzolite of the Cao Bang complex (Hoa, 2007). To the northwest of the Song Hien structure, two-mica granite of the Late Cretaceous Pia Oac complex, with which greisen-type W–Sn mineralisation is associated, is widespread (Vladimirov et al., 2012). Mafic and silicic magmatic rocks, forming typical Permian–Triassic volcano-plutonic associations, are distributed along the Cao Bang–Tien Yen fault system (Hoa et al., 2008).

Numerous gold deposits are exposed in the Song Hien rift; these can be divided into two types based on the ore-hosting rocks: (i) carbonaceous sediment-hosted Au–As; and (ii) gabbroid-hosted Au–As–Sb mineralisation. The latter type is the subject of this study.

2.2. Deposit geology

The Hat Han gold deposit is located in the north of the Song Hien basin, between the Ha Giang and the Cao Bang provinces (Fig. 2). The deposit is hosted in a small (3.5 km^2) mafic intrusive body belonging to a gabbrodolerite–diabase association of the Early Triassic Cao Bang igneous complex (νT1cb).

The least altered rocks in the intrusion are sulphide-free quartz-bearing monzogabbros (Fig. 4A). They are coarse- to medium-grained, massive, with hypidiomorphic-granular textures and elements of granophyric and monzonitic textures. These rocks consist of clinopyroxene (20–30 vol.%), plagioclase (20–45 vol.%), hornblende (5–10 vol.%), K–Na feldspar (~10 vol.%), quartz (~10 vol.%), and biotite (3–10 vol.%). Apatite and titanite occur in minor amounts (1–2 vol.%). Magmatic Fe–Ti oxides (1–5 vol.%) are characterised by ilmenite and are interstitial to silicates. Clinopyroxene grains are subhedral to anhedral and range in size from 0.4 to 1.5 mm. Plagioclase occurs as subhedral to euhedral grains, ranging from 0.4 to 1.5 mm in length, and small euhedral laths enclosed by clinopyroxene. Hornblende grains are short-prismatic and range in size from 0.4 to 0.6 mm. K–Na feldspar occurs as subhedral to anhedral and aggregate grains, ranging from 0.4 to 1.0 mm, filling the interstices between plagioclase, clinopyroxene, and hornblende. Granophyric intergrowths of quartz and alkali feldspar are common. Quartz occurs as single anhedral grains, 0.2 to 1.2 mm in size, filling the interstices between silicates. Biotite grains 0.4 to 0.8 mm in size, are interstitial to other silicates, and sometimes enclose plagioclase and apatite grains. Apatite grains are euhedral and range from 1.0 to 1.2 mm in length.

The quartz-bearing monzogabbro surrounding the ore bodies is altered to varying degrees (Fig. 4A). Clinopyroxene is uralitised, chloritised, epidotised and locally carbonatised, often with the original grain shapes well-preserved. Hornblende is completely replaced by a fine-grained aggregate of epidote, zoisite, chlorite, and opaque minerals. Biotite is discoloured and is replaced by chlorite and cleavage-parallel opaque minerals. Plagioclase is completely saussuritised and chloritised, and is occasionally replaced by albite. K–Na feldspar is pelletised. The
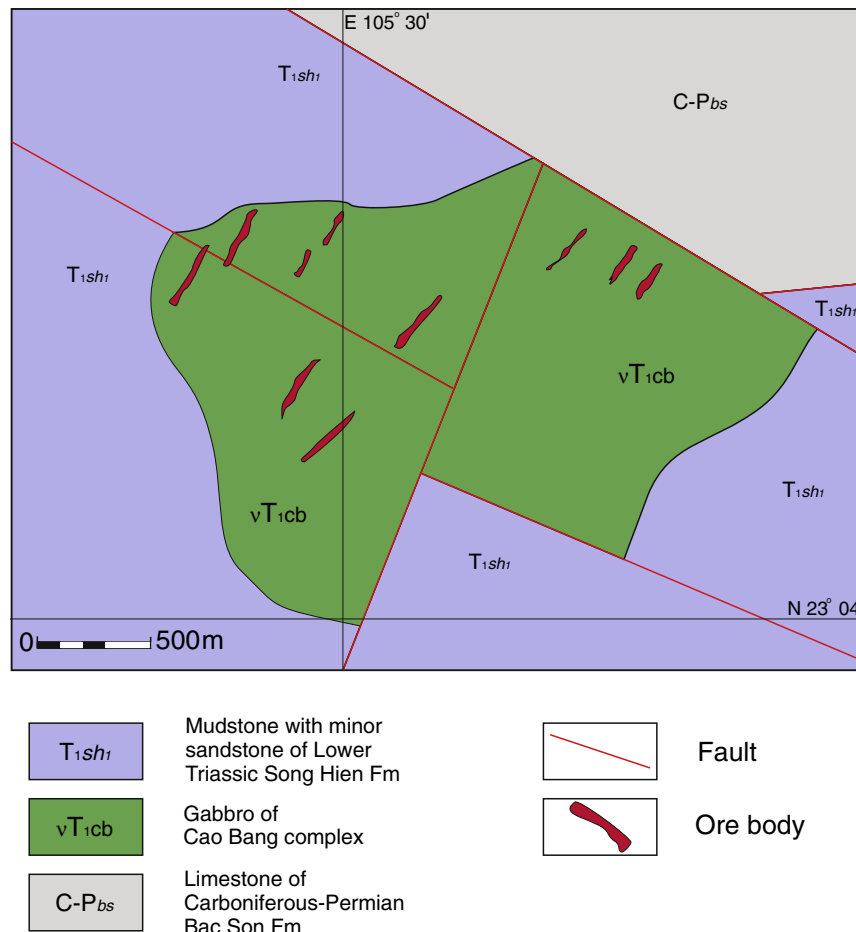

Fig 2. Geological map of the Hat Han deposit.

magmatic ilmenite does not show any alteration. No sulphides are observed.

The gold ore-hosting quartz-bearing monzogabbro is altered to sericite–chlorite–carbonate metasomatite containing sulphides (up to 30 vol.%), minor quartz (up to vol.5%), rutile (up to 2 vol.%), and muscovite (≤1 vol.%) (Fig. 4B–D). However, the original magmatic texture can be detected in the altered rocks (Fig. 4B). The carbonate (5 to 10–15 vol.%) occurs in the form of fine-grained aggregates within the fine-grained sericite–chlorite groundmass. The original magmatic ilmenite is commonly replaced by leucoxene, rutile, and titanite, and is locally altered to an intergrowth of rutile, chlorite, and sulphides. Sulphides occur as discrete grains. Several generations of veins, which are thin (up to 2 mm) and have various orientations, are observed in the altered rocks. The veins are sulphide-free and consist of carbonate (60–80 vol.%), quartz (10–30%), and alkali feldspar (~10%) (Fig. 4C–D). Both the sericite–chlorite–carbonate metasomatite and the veins locally show cross-cutting relations with the original magmatic minerals (altered Fe–Mg silicates, apatite).

The ore bodies comprise metasomatic and deformed zones up to 150–200 m in length, trending north-northeast. The width of the ore bodies vary from 2 to 3 to 50 m, whereas their height reaches 150 m. The gold content varies from 1 to 2 to 20 ppm.

In plan view, the deposit is visibly zoned both vertically and horizontally (Fig. 3). The central body consists of strongly metasomatic rocks. The ore sulphide contents increase with metamorphic grade, up to 30 wt.% in the centre of the ore body. Antimony mineralisation commonly occurs in the central part, characterised by massive antimony ore formed by aggregates of single stibnite minerals. Surrounding the massive stibnite are deformed (crushed) zones where gold-bearing metasomatite fragments are cemented in the gabbro by quartz and minor amounts of stibnite, and rarely by sphalerite. In some cases, gold-sulphide ores are cemented by stibnite compounds.

The sulphide content in the metasomatite decreases together with gold concentration from the centre to the margin of the ore body. It is also observed that the rate of the hydrothermal metasomatic process similarly decreases from the centre to the margin of the ore body.
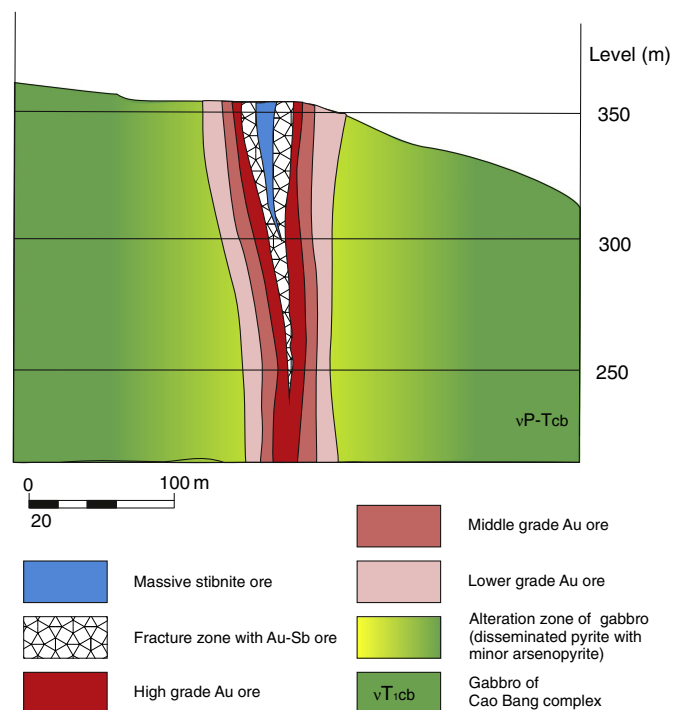

Fig. 3. Conceptual cross section of the Hat Han deposit.

Two cross-cutting veins systems are observed in the Hat Han ore deposit. The first vein system comprises quartz-carbonate veinlets up to 5 mm thick. In addition to from quartz and carbonate minerals, rare pyrite grains also occur in the vein mass. These veins cross-cut metamorphosed gabbro and formed by metasomatic alteration of the wall-rock.

The second vein system comprises milky quartz with variable quantities of ore minerals. The vein thickness varies from millimetres to meters. These quartz veins cut the quartz-carbonate veinlets and the gold-bearing metasomatite. Cementation by milky quartz veins containing gold-bearing metasomatite leads to the formation of breccia-type ore-bearing gold–antimony mineralisation. The veins lack gold ore fragments, with the milky quartz veins containing only antimony ore with small quantities of base metals. Genetically, the veins formed in the Hat Han ore deposit are not related to the gold-bearing ore.

3. Sampling and analytical method

Samples were collected from ores of the main zone. The mineral composition, textural–structural features, and mineral relations were studied under an optical microscope in reflected and transmitted light. A total of 50 polish sections were studied to characterise the mineralogy, as well as paragenetic and textural relationships. The monomineral fractions of sulphides were sorted out under a binocular microscope from heavy concentrates. The chemical composition of sulphides was analysed in polished samples on a Camebax-micro electron microprobe and on a JSM-6510 SEM equipped with EDS SSD INCA (OXFORD) at the Institute of Geology and Mineralogy in Novosibirsk, Russia. The experimental conditions are focused beam in spot mode, accelerating voltage at 20 kV, counting times at 10 s, and beam current at 50 nA. Arsenopyrite and pyrite were analysed for Fe, S, As, Au, Sb, Ni, Ag, Zn, Cu, and Co. The following sulphides and synthetic compositions were used as standards: FeS_2 (Fe, S), FeAsS (As), $Au_{0.75}Ag_{0.25}$ (Au, Ag), Sb_2S_3 (Sb), FeNiCo (Ni, Co), ZnS (Zn), and $CuFeS_2$ (Cu). Estimated detection limits were 0.036 wt.% for Ni, 0.03 wt.% for Co, 0.025 wt.% for Fe, 0.05 wt.% for As, 0.012 wt.% for S, 0.045 wt.% for Ag, 0.037 wt.% for Sb, and 400 ppm for Au.

The gold contents in the sulphides were determined by a Perkin-Elmer 3030 Zeeman Atomic Absorption Spectrophotometers (AAS) at the Institute of Geology and Mineralogy, Novosibirsk, Russia. Precision and accuracy were based on the analyses of the geological standard SZH-3.

Ag, Cu, Pb, Zn, W, and Tl were analysed by ICP and ICP-MS (multi-acid digestion), Au, As, Sb, and Hg by INAA. Chemical analyses were carried out by Activation Laboratories Ltd., Canada. Detection limit were 1 ppb for Au, 10 ppb for Hg, 0.1 ppm for Sb, 0.2 ppm for Cu, 0.05 ppm for Tl and Ag, 0.5 ppm for As, Pb, and Zn, and 1 ppm for Mo and W.

Sulphur isotope compositions were obtained from twelve samples of pyrite and ten samples of arsenopyrite. The isotopic composition of sulphur in sulphides was analysed at the Analytical Center of the Institute of Geology and Mineralogy, Novosibirsk, Russia. The isotopic composition of sulphur is expressed as $\delta^{34}S$ unit, in per mil (‰), relative to Canyon Diablo Troilite standard, and its analytical precision is about ±0.2‰.

4. Results

4.1. Mineral composition and ore structure

The Hat Han deposit is a complex-type ore deposit, which is significant because it contains both gold and antimony. There are three ore types: gold, antimony, and their compound. The third compound type was produced by the combination of the two early mineralisation types. Aside from their presence in one useful compound or another, the three ore types differ in formation structure and mineralogical composition.
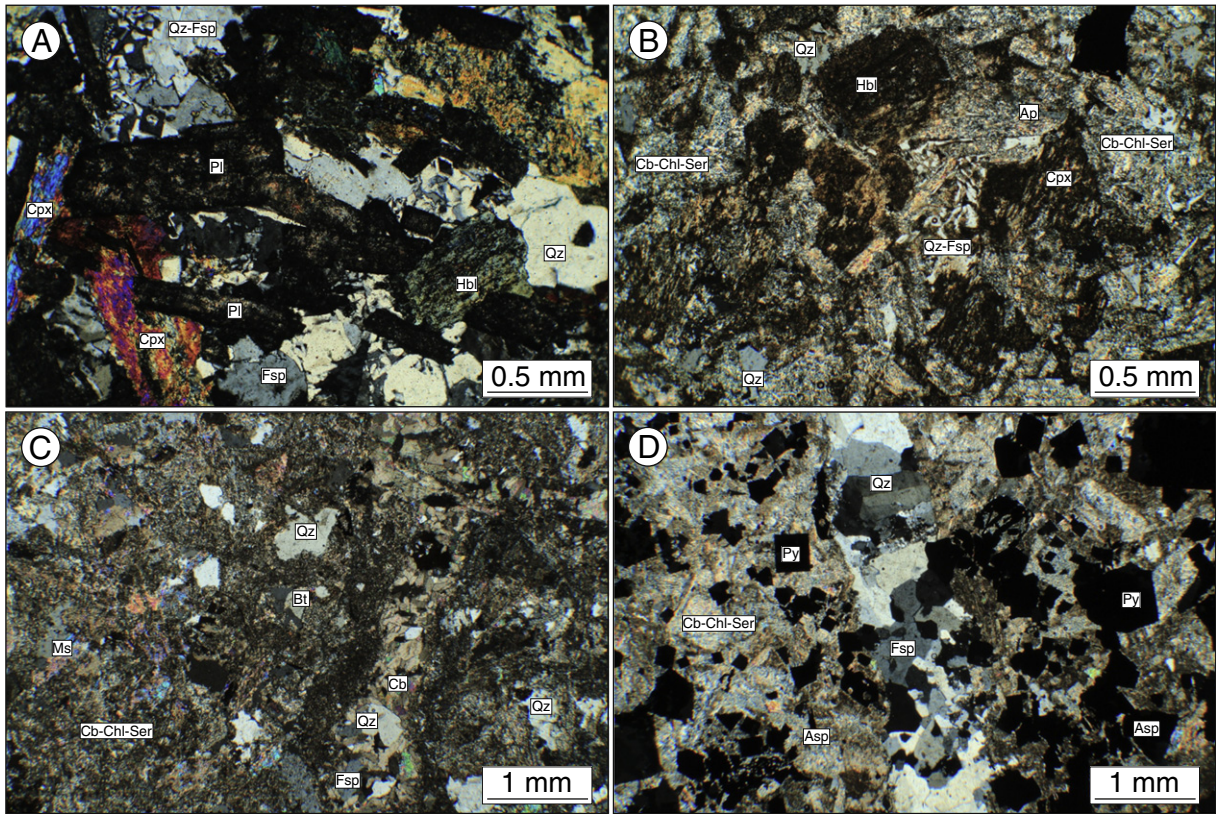
Fig. 4. Photomicrographs (transmitted light, cross-polarized) showing the mineral assemblages of the mafic host rock: (A) unaltered quartz-bearing monzogabbro; (B, C) altered quartz-bearing monzogabbro; (D) altered quartz-bearing monzogabbro with pyrite and arsenopyrite. Trend from A to D show process of alteration mafic host rock. Mineral abbreviations: *Qz = quartz, Fsp = K–Na feldspar, Pl = plagioclase, Cpx = clinopyroxene, Hbl = hornblende, Cb = carbonate, Chl = chlorite, Ser = sericite, Ap = apatite, Bt = biotite, Ms = muscovite, Py = pyrite, Asp = arsenopyrite.*

Ore structures at the Hat Han deposit are complex (heterogeneous); however, massive, breccia-type and disseminated are the most common. The massive structure is characteristic of the central part of the deposit where antimony ore is dominant. Elsewhere massive antimony aggregates form ore packages with thicknesses up to 0.5–1 m.

The disseminated structure is most characteristic of the gold-sulphide ores. The ore mineral dissemination rate decreases from the central to the marginal ore body. In the central part of the ore body, where gold-sulphide ores are less deformed, ore content may increase up to 30–40 wt.%; in contrast, ore content decreases to 1–3 wt.% in the marginal parts of ore body. This structure type is characterised by randomly distributed ore mineral grains within the host rock. In some cases, disseminated gold-sulphide ores are cut by small veins, consisting mostly of pyrite, to form a vein-diffused-type structure.

The breccia-type structure is typical of the complex ore type, which contains economic quantities of gold and antimony. The cement in breccia-type ore is quartz and stibnite, where the latter increases significantly towards the centre of the ore body. The fragments in this ore structure are mostly ore-bearing altered gabbro with various degrees of sulphidisation.

The mineralogical composition of the antimony ore is simple, containing aggregates of massive stibnite.

The gold ore in the metasomatic altered gabbro consists of paragenetic associations of arsenopyrite and pyrite, with minor amounts of sphalerite and rutile. The gold ore in the Hat Han deposit is high grade; however, no native gold has ever been discovered there.

The complex ore shows the most diverse mineralogical composition. In ore-bearing quartz veins and breccia (depending on the cement/fragment proportions), the main ore minerals are arsenopyrite, pyrite, stibnite, and in some cases sphalerite. In addition, the quartz vein-type ore also contains tetrahedrite, zinkenite, and chalcopyrite minerals.

The proportions of pyrite and arsenopyrite vary widely. Pyrite is commonly the most abundant mineral; however, the gold concentration is dependent on the quantity of arsenopyrite. In gold-rich ores (Au >10 ppm), the arsenopyrite content may be as high as 50 wt.% of all the sulphide minerals.

Pyrite and arsenopyrite show very similar textural features. They occur as euhedral grains with sizes from 0.05 to 0.5 mm (Fig. 5A–D). This association sometimes also includes rutile, characterised by elongate and euhedral grains replacing ilmenite in the host gabbro. Aggregates of crushed pyrite and arsenopyrite are cemented by massive stibnite (Fig. 5E–F).

The pyrite contains 0.9 wt.% and 1.4 wt.% of Ni and As, respectively. The average As concentration, determined from 110 EPMA analyses, is 0.34 wt.%. Whereas, the average Sb, Ni, and Co concentrations in arsenopyrite, determined from 100 EPMA analyses, are 0.7 wt.%, 0.15 wt.% and 0.87 wt.%, respectively. The average chemical compositions of the pyrite and arsenopyrite are shown in Tables 1 and 2.

Mineralogical surveys at the Hat Han deposit have not yet found native gold in its independent mineral phase form; therefore, evaluation of gold concentration in sulphide phases is essential. The results of electron probe microscopic analysis (EPMA) show that the pyrite contains up to 1700 ppm of gold, whereas in arsenopyrite the concentration is 3100 ppm. The EPMA detection limit is 400 ppm.

The relation between Au, Sb, and major arsenopyrite constituents (As, S, Fe) was also analysed. The compositional concentration relationship of the above elements is illustrated in Fig. 6, revealing that gold content in arsenopyrite increases with increasing As content. Fig. 6 also shows a weakly negative correlation between Au and S concentration. Elemental pairs of Fe–Au and Sb–Au are not correlated.

The high concentration of Au in pyrite appears to be independent of the major elements (e.g. Fe and S), Sb, and As (Fig. 7). A weakly positive
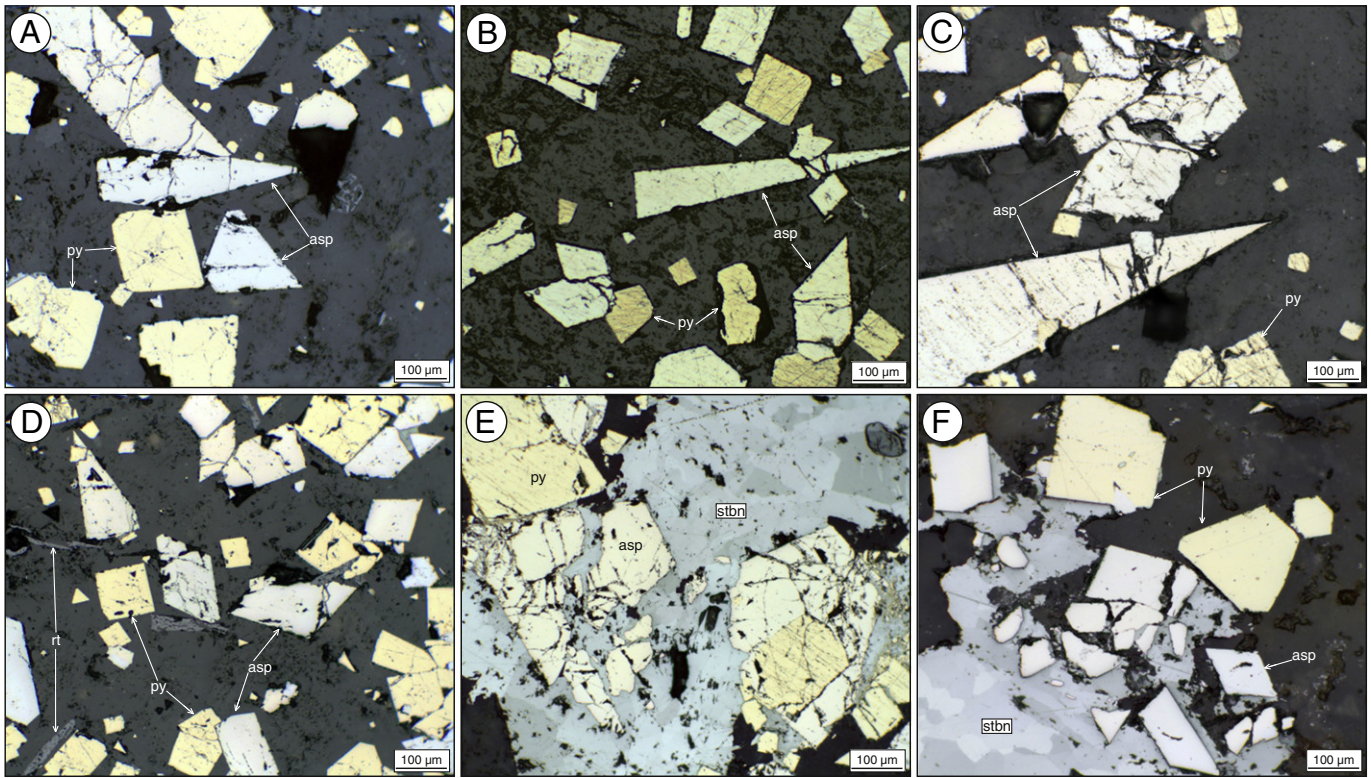
Fig. 5. Photomicrographs (reflected plane polarized light) showing the mineral assemblages in different types of ore in the Hat Han deposit. A, B, C, D — Au ore: disseminated euhedral grains of pyrite and arsenopyrite and elongated grains of rutile in mafic host rock; E, F — Complex (Au–Sb) ore: crashed grains of pyrite and arsenopyrite cemented by massive stibnite. Mineral abbreviations: *Py = pyrite, Asp = arsenopyrite, Stbn = stibnite; Rt = rutile.*
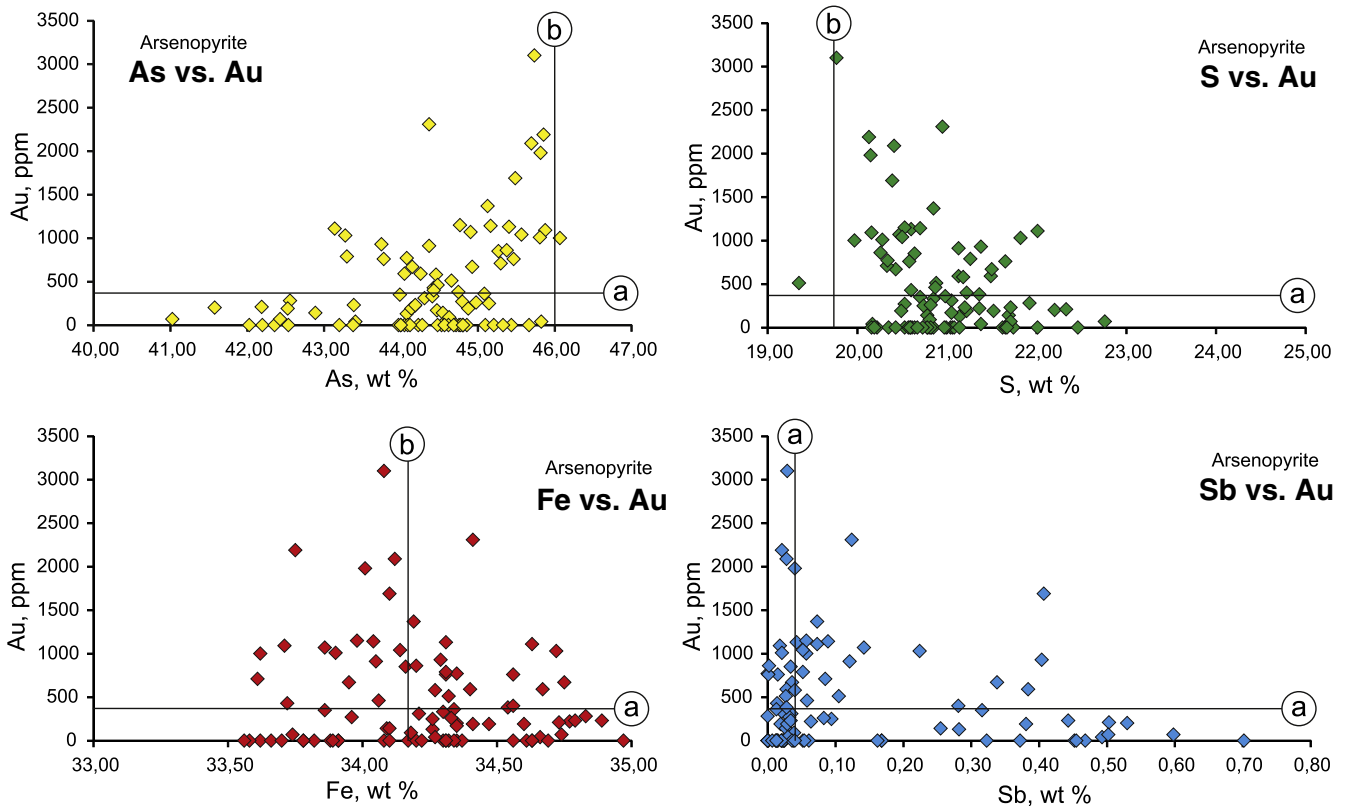
Fig. 6. Relationship of gold content in arsenopyrite from the concentration of the main and trace components. Line a — detection limit, b — theoretical composition.
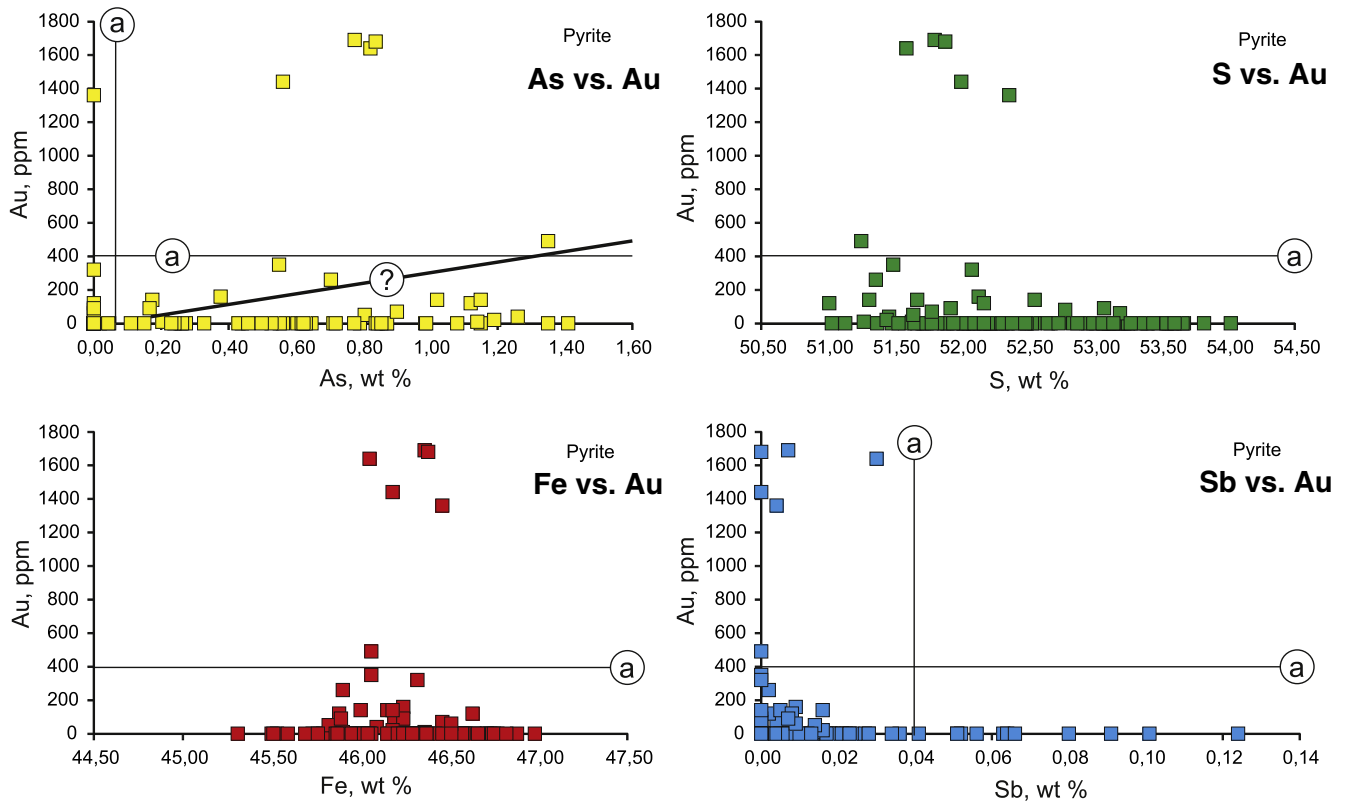
Fig. 7. Relationship of gold content in pyrite from the concentration of the main and trace components. Line a — detection limit, ? — hypothetical line of depending on the contents Au and As.

correlation between Au and As concentration in pyrite is observed; however, the elemental concentrations are equal to or lower than the detection limit. This analytical method, therefore, may be used as supporting evidence.

4.2. Geochemistry

The geochemical characteristics of a gold ore are expressed by the relationship between the concentrations of gold and other accompanying elements in the ore. This expression is an important indicator of a given deposit. For example, sediment-hosted gold deposits in black shale formations are characterised by Au, As, and Sb association

Fig. 8. Chondrite-normalised rare-earth element.
Data for the Ban Giem and Nguyen Binh are from Hoa, 2007.

(Novozhilov and Gavrilov, 1999). The most important feature of this mineralisation type is the close relationship between Au and As, and Sb to a lesser extent. The significant feature of Carlin-type (U.S.A.) and Carlin-like deposits in southwestern China is Au, As, Sb, Hg and Tl association (Chen et al., 2011; Peters et al., 2007; Zhang et al., 2005). Therefore, with the aim of clarifying the geochemical characteristics of gold mineralisation in the Hat Han deposit, the trend and the relation between Au and accompanying elements in ore components, ore samples were collected and analysed for geochemical composition at Actlabs Ltd. (Ontario, Canada). Various ore, host, and unaltered gabbro samples were analysed for the abundances of 60 elements. Au concentrations were analysed in the black shale from the Early Triassic Song Hien formation, overlying the gold–sulphide host gabbro.

According to the latest ICP analytical results, the ore elemental concentrations in the gabbro-hosted ore bodies are insignificant. The major characterising element compositions of the ore samples are given in Table 3. The gold content in the black shale overlying the gabbro is −46 ppb.

4.2.1. Host rock geochemistry

The major and trace element compositions of the Hat Han gabbro are shown in Table 4. The gabbro is characterised by low TiO_2 (=0.3–1.8 wt.%), MgO (4 wt.%), and low P_2O_5 (=0.16–0.22 wt.%); relatively low total alkalis ($Na_2O + K_2O = 3.5$ wt.%) and Na_2O/K_2O ratio ~1. The gabbro contains relatively low Cu (24.8 ppm), Ni (14.7 ppm), Co (42.7 ppm), and Cr (1 ppm); high V (116 ppm); and high Rb (87.9 ppm), Th (9.6 ppm), Ce (48 ppm), Zr (38 ppm), and the rare earths, especially the light elements (LREE). The chondrite normalised rare earth element pattern of the Hat Han gabbroids, showing characteristic Eu minimum, is closely similar to that of the Ban Giem and Nguyen Binh massif (e.g. Hoa, 2007; Fig. 8). The primitive mantle-normalised trace element pattern is also closely analogous to that of
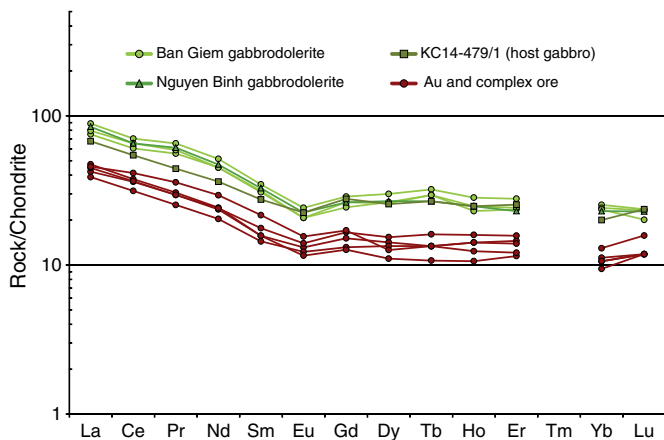
Stage / Mineral	Pre-ore magmatic	Gold Ore metasomatic	Antimony Ore quartz-vein
Clinopyroxene	●		
Plagioclase	●		
Hornblende	●		
Biotite		●	
K-Na feldspar		●	●
Quartz	○	○	
Ilmenite	○		
Apatite	○		
Chlorite		●	
Epidote		●	
Saussurit		●	
Secondary amphibole		○	
Zoisite		○	
Albite		○	
Sericite		●	
Carbonate		○	
Titanite		○	
Leucoxene		○	
Rutile		○	
Arsenopyrite		●	
Pyrite		●	
Sphalerite		○	
Milky quartz			●
Tetraedrite			○
Zinkenite			○
Chalcopyrite			○
Stibnite			●

Fig. 9. Paragenetic sequence of mineralisation and alteration in the Hat Han deposit.

the Ban Giem and Nguyen Binh gabbros in the Cao Bang igneous complex (e.g. Hoa, 2007). However, the REE concentrations in the Hat Han gabbro are lower compared to the Ban Giem and Nguyen Binh gabbroids (Fig. 8).
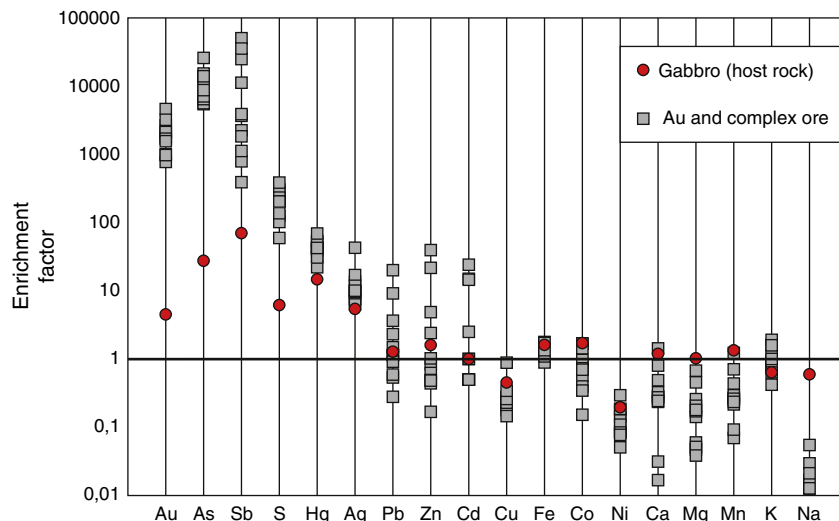
4.2.2. Ore geochemistry

The antimony ore is characterised by a high concentration of Sb (KC483/8, KC488; Table 3). Ores in quartz veins, stibnite, and base metal ore-bearing crushed zones contain high concentrations of Pb and Zn, up to 1000–3000 ppm. The gold concentrations in the antimony ores vastly depend on the presence and quantity of fragments that contain early phase gold-bearing sulphide minerals. Gold contents varying from zero to 2 ppm are closely associated with As concentrations.

Au in the disseminated gold ores varies from 4 to 12 ppm. As concentrations in these ores are relatively high, with an average of ~2 wt.%. Gold content in the disseminated ores, like that of the antimony ores, is directly dependent on arsenic content in the ore. The average concentration of Sb in the disseminated gold ores is 1000 ppm (Table 3). The Sb–Au complex ores show geochemical characteristics in the range between the above-described two ore types.

4.3. Sulphur isotopic composition

The analytical results for the sulphides are listed in Table 4.

The $\delta^{34}S$ values from five arsenopyrite samples range from 6‰ to 9.2‰ (mean value = 7‰). Sulphur isotopic compositions of pyrite range from 6‰ to 7.9‰ (mean value = 7‰); of stibnite are low, ranging from 0.3‰ to 6.6‰ (mean value = 3.7‰); and of diagenetic pyrite yield a value of 7.3‰. The data show the following salient features.: (i) the pyrite and arsenopyrite are commonly paragenetic, having similar sulphur isotopic compositions; in contrast, the stibnite is characterised by high ^{32}S; (ii) the sulphur isotopic variation between samples does not depend on gold concentration, the presence of late antimony mineralization, and the concentration of Au in sulphide; and (iii) there is a systematic enrichment of light sulphur isotopes in pyrite-arsenopyrite-stibnite. This decreasing trend is in accordance with equilibrium fractionation of sulphur isotopes during the precipitation of sulphides (Chen et al., 2015a).

5. Discussion

5.1. Ore-forming process and paragenetic sequence

The ore is characterised by massive, breccia-type and disseminated structures. According to the mineral intercalation relationships, the mineral formation sequence had three stages (Fig. 9). From earliest to latest, the three stages can be classified as: (i) pre-ore magmatic, (ii) gold ore metasomatic, and (iii) antimony ore quartz-vein. Gold-bearing sulphides

Fig. 10. Element enrichments in gold ore of the Hat Han deposit (grey squares) relative to those of unaltered host gabbro (red circle).

(mainly arsenopyrite) were formed during the second stage, whereas antimony ore was formed during the final stage. The paragenetic sequence of the Hat Han deposit is shown in Fig. 9. The observations that were used to define these three sequential stages are as follows.

5.1.1. Pre-ore magmatic stage

This stage is not directly related to ore formation; however, a study of the mineral composition of non-metamorphosed rocks allows determination of the metasomatic process stages. Moreover, the magmatic rocks are a source of Fe, necessary for sulphide concentrated Au formation. Co-existing mineral associations formed during the magmatic stage include clinopyroxene, plagioclase, hornblende, biotite, K–Na feldspar, quartz, apatite, and ilmenite.

5.1.2. Gold ore metasomatic stage

This stage is characterised by intensive alteration of the host rocks, filtering out a series of rock-forming elements while introducing ore elements.

Two major alteration types can be recognised at the Hat Han deposit: (i) propylitic, and (ii) sericitic. Propylitic alteration denotes assemblages, including chlorite, epidote, zoisite, saussurite, albite, and secondary amphibole, which have been formed by alteration of the original magmatic silicates. No sulphides have been observed in the propylitised rocks. As for sericitic alteration, the coexistence of sericite, chlorite, sulphides, carbonate, quartz, rutile, and carbonate–quartz–alkali feldspar veins indicates simultaneous sericitisation, chloritisation, sulphidation, and carbonatisation, with minor silicification and feldspathisation. This alteration type is the main stage of gold-bearing sulphide mineralisation at the Hat Han deposit. Propylitic alteration is developed to varying degrees in magmatic rocks, both surrounding the orebodies and within the orebodies, whereas sericitisation is intense within the orebodies.

During sericitisation, ore mineralisation occurs, including widespread gold-bearing pyrite and arsenopyrite and minor amounts of sphalerite and rutile. The formation of pyrite and arsenopyrite occurs as Fe is expended from earlier-formed Fe-bearing minerals, such as coloured and accessory minerals in gabbro. A surplus of titan, formed by replacement of ilmenite, leads to the formation of secondary rutile in metasomatites. The relationship between the main ore minerals (e.g. pyrite and arsenopyrite) and rutile suggests their contemporaneous formation. This relationship provides mineralogical evidence that sulphide-forming processes occur as a result of the replacement of Fe-bearing minerals in host rocks.

5.1.3. Antimony ore quartz-vein stage

Formation of co-existing ore minerals during the quartz-vein stage commenced during the crushing process of the earlier-formed gold ore in altered gabbro. Hydrothermal solution may occur in crushed zones, forming ore breccia with gold ore fragments cemented by milky quartz veins containing variable quantities of ore minerals. These processes may lead to the formation of the complex gold–antimony ore at the Hat Han deposit.

Formation of ore minerals may begin with tetrahedrite, zincite, sphalerite, and rare chalcopyrite, followed by stibnite. At the end of this mineralisation stage massive antimony ores were formed.

5.2. Possible sources of ore elements

The majority of the gold deposits in the Song Hien depression are terrigenous (black shale) sediment-hosted deposits. A series of world-class gold deposits, termed the "golden triangle", have long been known in the Triassic Nanpanjang rift basin (China), north of the Song Hien depression, and have been studied and described in detail (Chen et al., 2011, 2015a,b; Peters, 2002; Peters et al., 1998, 2007; Zhou et al., 2002; Zhong et al., 2002). These deposits are embedded predominantly in Triassic, and some in Devonian, sediments. However, there
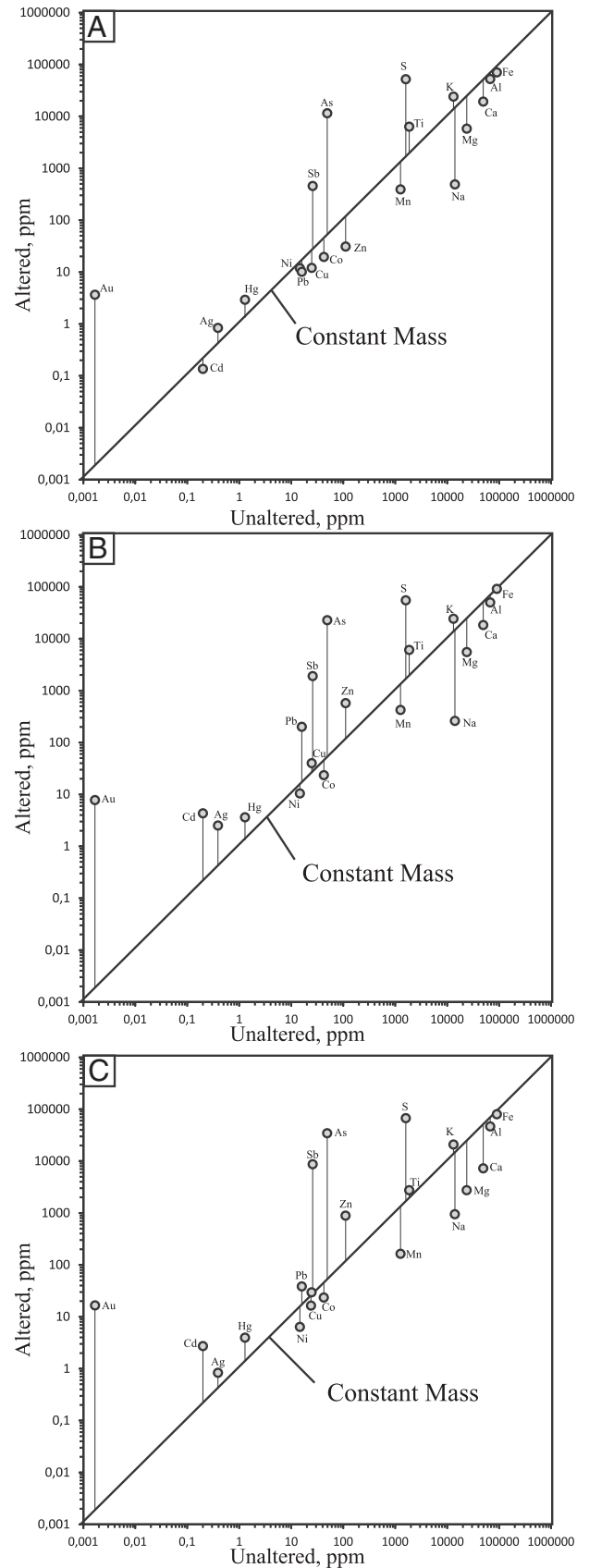

Fig. 11. Isocon diagrams showing element mobility in ore with different gold content: (a) to 4 ppm; (b) 4 to 10 ppm; (c) up 10 ppm. Elements that plot above or below the isocon are, respectively, introduced or depleted. In each plot, the immobility of Fe and the introduction of S and Au are clear evidence of gold precipitation by sulphidation of host-rock iron.

are examples showing that some mafic magmatic rock-hosted deposits have similar mineralogical and geochemical characteristics to the sediment-hosted. In Nevada, mafic rocks are known to contain Carlin-type sediment-hosted Au deposits at the Twin Creeks deposit (Bloomstein et al., 1991; Thoreson et al., 2000) where basalt is the host rock, and at the Betze deposit where lamprophyre and diorite are the ore host rocks (Leonardson and Rahn, 1996; Peters et al., 1998). In the "golden triangle", the Jimba, Badu, and Anna deposits are hosted by gabbro and diabase rocks (Dong et al., 2014; Li et al., 2014; Peters, 2002; Peters et al., 2007). Studies by Chen et al. (2011, 2015a,b), Peters et al. (2007), Zhou et al. (2002), and Zhong et al. (2002) provide details of the ore geochemical characteristics, which show that the source rocks supplying the sulphur and ore elements in the mineralisation process to form these deposits are terrigenous sediments.

Sb–Au mineralisation at the Hat Han deposit is hosted in altered mafic rocks. It is unlikely that these host rocks supplied the sulphur and ore elements required for arsenic-type gold mineralisation. The trace element compositions shown above may explain the behaviour of some characteristic elements during the ore deposit formation. An indication of the mass transfer associated with gold mineralization can be obtained by dividing the average trace element concentrations in the ores by the average trace element concentrations in the crust (Clark values) to obtain the enrichment factors. In Fig. 10, the trace elements are arranged from the Carlin suite (Tl, Hg, Sb, As and Au) on the left, through Ag and base metals (Pb, Zn, and Cu) to Mo and W on the right.

Three elemental groups may be categorised as follows: (i) those introduced during the ore formation process; (ii) elements removed during ore formation; and (iii) elements whose concentrations are unchanged or vary insignificantly. The first group includes Au, As, Sb, and S, as well as Ag and Hg although their concentrations did not increase noticeably. The formation of the gold-bearing altered mafic rock environment occurred following the input of Au, As, Sb, and S. Compared to the unaltered gabbro, the concentrations of the above elements in metasomatite increase three fold.

During the ore formation process, Ca, Mg, Mn, and Na are removed from the metasomatised zone, possibly due to the replacement of plagioclase and melanocratic minerals in gabbro. Inert behaviour may include Pb, Zn, and Cd, although their low and high presence in ore minerals compared to unaltered rocks may simply be explained by their redistribution in various ore types. Concentrations of Cu, Ni, and Co in gabbro decrease during the ore formation process, whereas K and Fe remain mostly unchanged.

The unchanged concentration of Fe during the formation of gold ore suggests that ore mineralisation occurs as the result of sulphidation of the host gabbro, where sulphide minerals are formed by taking (borrowing) iron from the gabbro. This process may explain the formation of sediment-hosted gold deposit, including Carlin-type deposits (Large et al., 2011; Peters et al., 2007; Su et al., 2009).
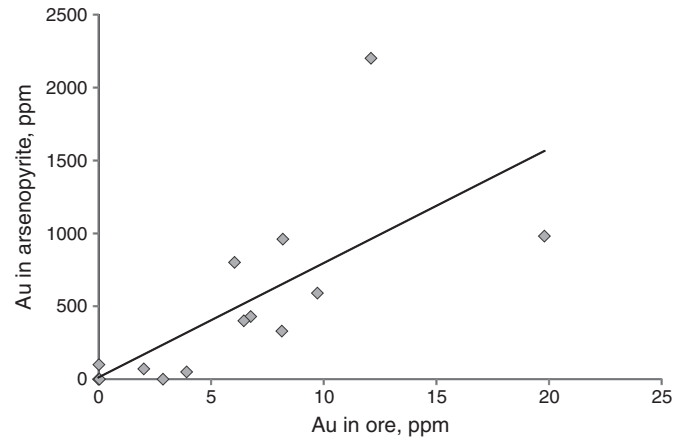
Fig. 13. The relationship of gold content in arsenopyrite from the concentration in ore.

Isocon diagrams additionally provide a graphical expression of component loss and gain. Grant (1986) demonstrated that isocon diagrams can be used to calculate gain or loss of major, minor, and trace elements due to alteration. This graphical method is based on the equations of Gresens (1967). Logarithmic isocon diagrams have previously proven useful in studies of mass transfer in Carlin-type systems (Hofstra and Cline, 2000) and are subsequently used here.

ICP analytical results show three isocon diagrams for different groups with vastly different gold concentrations. The first isocon diagram is constructed for ore-bearing gold with concentration of ≤4 ppm (Fig. 11A), the second diagram shows the ore group with concentrations from 4 to 10 ppm (Fig. 11B), and the third diagram shows the ore group containing ≥10 ppm (Fig. 11C).

Analysis of the isocon diagrams for the ores with various gold concentrations shows that As content typically increases with increasing Au content. This behaviour of arsenic is due to the fact that arsenopyrite becomes a major concentration of gold in the ores. Increasing concentration of As together with Au may explain the deposit formation (structure). As depicted in the schematic cross-section across the ore body (Fig. 3), the most enriched gold-containing ore is concentrated close to the central part of the ore body. Arsenic-bearing ore is similarly concentrated close to the axial part, forming zones of crushed and quartz veins. In the central part of the ore body, ore breccia is frequently observed, with cement consisting of quartz-antimony matrixes, and fragments composed of altered gabbro with abundant gold-bearing arsenopyrite impregnations.

Mercury, like antimony and arsenic increases with increasing gold concentration. Zinc and cadmium are ore elements whose concentrations vary with increasing gold content in the ore. For ore containing ≤4 ppm gold (Fig. 11A), concentrations of the above elements are lower than those in the host rocks. This behaviour may be explained
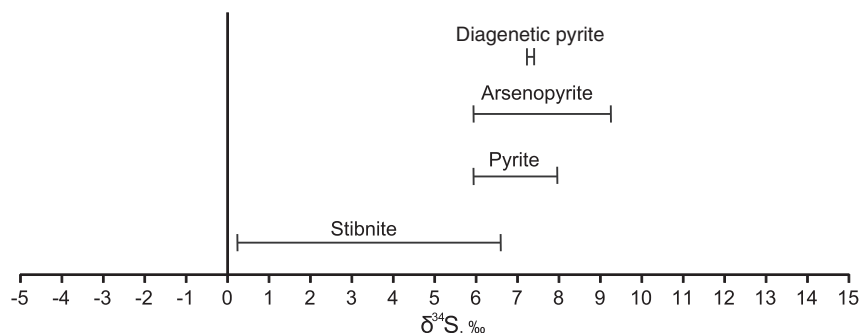
Fig. 12. Plot of $\delta^{34}S$ of sulphides from the Hat Han deposit.
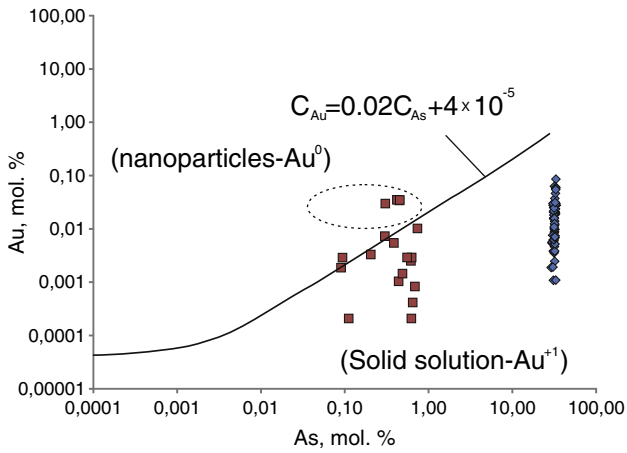
Fig. 14. The relationship between the solubility limit of Au and As a function of arsenic content in pyrites according to Reich et al. (2005). Plotting all the composition data of Au and As in mole percent (mol.%) of pyrites from the Hat Han deposit indicates that most of Au in pyrites and arsenopyrites maybe occur as chemically bound (Au$^+$), and a small fraction as native nanoparticles (Au^0), see the text for details.

by the spatial redistribution of these elements between zones with different degrees of alteration. For ore containing Au concentrations from 4 to 10 ppm, these element concentrations are rarely increased and higher than their contents in the most enriched ores. This regulation is related to the uneven redistribution of sphalerite in ores. Silver content is increased in ore; however, its concentration is not directly related to gold content. As a consequence, this suggests that partial concentration of silver in ore is related to the concentrations of galena and tetrahedrite.

Indeed, concentrations of major rock-forming components are unchanged in ores with different gold content. Elements removed from

rocks by ore fluids include Mg, Ca, Na, and Mn (Fig. 11A-C). This elemental behaviour is explained by the decomposition of plagioclase and coloured minerals. Generally, Al and Fe are viewed as immobile elements. The immobility of Fe and the introduction of S, Au, As, Sb, and Hg, evident on the isocon diagrams, require that Au- and trace element-rich sulphides in the ore precipitated where H_2S in ore fluids reacted with Fe-bearing minerals in the host rocks (Hofstra et al., 1991; Saunders et al., 2014). Concentrations of Ti to a lesser extent, are increased in the sericitic altered orebodies. An increase in potassium is due to sericitisation occurring as a direct result of weak to moderate potassic metasomatism. The distributions of major elements Ti and S in orebodies reflect alteration, particularly sericitisation, sulphidation and formation of Ti oxides (mainly rutile).

5.3. Possible sources of sulphur

The sulphur isotopic compositions vary within a narrow range, with an average $\delta^{34}S$ of 7‰, although light isotopes show accumulation tendency in later sulphidation periods (Fig. 12). Recent studies (e.g. Chang et al., 2008; Chen et al., 2015a; Large et al., 2007, 2011; Peng et al., 2014; Peters et al., 2007; Zhang et al., 2005) have shown that the source of sulphur supply to sediment-hosted gold deposits, including Carlin-type deposits, is the host sedimentary formation. In many cases, the sulphur isotopic compositions are dependent on the ages of the host rocks (Chang et al., 2008); however, this dependence is not commonly observed in magmatic hosted deposits. According to the above-compiled data, sulphur may be introduced by hydrothermal fluids rather than taken (borrowed) from gabbro.

Fig. 12 shows that the $\delta^{34}S$ value of arsenopyrite is identical to that of diagenetic pyrite in the sedimentary rocks. This similarity in the $\delta^{34}S$ values of arsenopyrite and diagenetic pyrite requires a sedimentary source (diagenetic pyrite and/or sulphur in organic matter within the sedimentary host rocks) as the major component contributing to the hydrothermal sulphide.
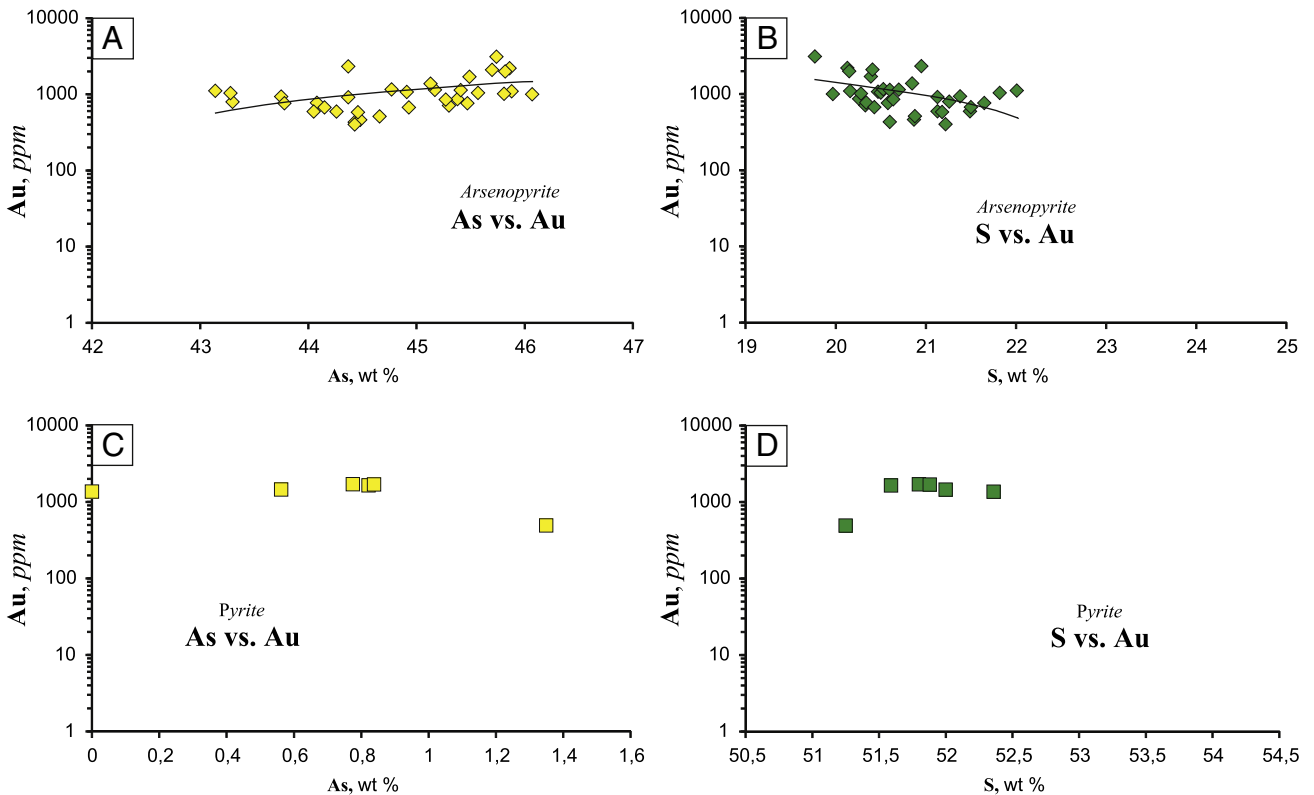
Fig. 15. As vs. Au (a), S vs. Au (b) for arsenopyrite and As vs. Au (c), S vs. Au (d) in pyrite diagrams. Plots indicate weak positive correlation As vs. Au and weak negative correlation S vs. Au in arsenopyrite of the Hat Han deposit. Whereas in pyrite such correlation is absent. The plot shows only data above the limit of detection EPMA.

The geology of the Song Hien rift basin comprises a Devonian–Triassic lithological sequence, where $\delta^{34}S$ in sulphide in equilibrium with sea water during these periods is estimated to vary between $+30‰$ and $+12‰$ (e.g. Holse et al., 1996). Initially, hydrothermal fluids rich in heavy sulphur isotopes circulating through low-pressure crushed zones are enriched by ore elements extracted from sediments by fluid-rock interaction. Subsequent interaction with sedimentary rocks causes the reduction of sulphate to H_2S by sulphate reduction with organic substances. The formation of H_2S results in enrichment of light ^{32}S. As hydrothermal fluid moves through crushed zones to enter the gabbro, under the effect of physic-chemical change, gold-sulphide ore begins to form. This instant sulphide is characterised by slightly positive $\delta^{34}S$ value. A similar model of isotopic variation in hydrothermal fluids relative to host rocks has been applied to explain some Carlin-like deposits in China (Chen et al., 2015a).

5.4. Gold-bearing sulphides

One of the distinct features of orogenic sediment-hosted gold deposits is the high concentration of gold in arsenic pyrite and arsenopyrite (widespread gold-bearing iron sulphides) (Peters et al., 2007; Reich et al., 2005; Simon et al., 1999; Yang et al., 1998). In many gold deposits, while lacking in native gold, this is the major form of gold existence (Ashley et al., 2000; Genkin et al., 1998). The appearance of 'visible' native gold was explained as a result of overlapping thermo-tectonic events and ore metamorphism (Large et al., 2007; Su et al., 2008).

Table 1
Electron probe microanalysis results (Au — ppm, other element — wt.%) for arsenopyrite from the Hat Han deposit.

Samp. no	Fe	Co	Ni	As	Au	S	Ag	Sb	Zn	Cu	Total
Detection limit	0.025	0.030	0.036	0.050	400	0.012	0.045	0.037	0.047	0.040	
KC14-481	34.26	–	–	44.08	130	21.14	–	0.28	–	–	99.78
KC14-481	34.72	–	–	43.28	1030	21.82	–	0.22	–	–	100.14
KC14-481	34.77	–	–	44.18	220	21.36	–	0.06	–	–	100.41
KC14-481	34.21	–	–	44.31	310	21.05	–	0.04	–	–	99.65
KC14-484	34.83	–	–	42.56	280	21.92	–	–	–	–	99.39
KC14-484	34.66	–	–	43.41	–	21.38	–	0.49	–	–	99.94
KC14-496	34.16	–	–	45.27	850	20.64	–	–	–	–	100.19
KC14-496	33.61	–	–	45.30	710	20.33	–	0.09	–	–	99.40
KC14-496	33.71	–	–	45.88	1090	20.16	–	–	–	–	99.89
KC14-496	34.31	–	–	45.47	760	20.58	–	–	–	–	100.45
KC14-478/2	33.62	–	–	46.07	1000	19.97	–	0.06	–	–	99.83
KC14-478/2	33.86	–	–	44.91	1070	20.47	–	0.14	–	–	99.50
KC14-478/2	34.29	0.11	–	43.75	930	21.38	–	0.40	–	–	100.03
KC14-478/2	34.31	–	–	45.41	1130	20.60	–	0.04	–	–	100.47
KC14-478/3	33.98	–	–	44.77	1150	20.53	–	0.06	–	–	99.45
KC14-478/3	33.90	–	–	45.81	1010	20.28	–	–	–	–	100.13
KC14-478/3	34.14	0.11	–	45.57	1040	20.50	–	0.05	–	–	100.47
KC14-478/3	34.20	–	–	45.38	860	20.26	–	–	–	–	99.94
KC14-479/4	34.56	–	–	43.97	–	21.06	–	–	–	–	99.62
KC14-479/4	34.17	–	–	44.53	–	20.83	–	0.04	–	–	99.58
KC14-479/4	34.37	–	–	44.76	–	20.59	–	–	–	–	99.74
KC14-479/4	34.31	–	–	44.81	–	20.35	–	–	–	–	99.48
KC14-480/2	34.67	–	–	44.26	590	21.49	–	0.38	–	–	100.90
KC14-480/3	34.75	–	–	44.15	670	21.50	–	0.34	–	–	100.83
KC14-480/3	34.31	–	–	43.30	790	21.26	–	0.05	–	–	99.00
KC14-480/3	34.73	–	–	42.19	210	22.33	–	0.50	–	–	99.81
KC14-480/3	34.40	–	–	44.05	590	21.13	–	–	–	–	99.69
KC14-480/4	34.63	–	–	43.14	1110	22.01	–	0.07	–	–	99.98
KC14-480/6	34.19	0.16	–	45.13	1370	20.85	–	0.07	–	–	100.55
KC14-483/2	34.60	–	–	44.14	190	21.52	–	–	–	–	100.30
KC14-483/2	34.05	0.87	0.10	44.37	910	21.13	–	0.12	–	–	100.74
KC14-483/2	34.10	–	–	44.55	140	20.78	–	–	–	–	99.47
KC14-483/2	33.96	–	–	44.80	270	20.53	–	–	–	–	99.41
KC14-483/3	34.22	–	–	44.09	–	20.85	–	0.05	–	–	99.23
KC14-483/3	34.18	–	–	44.63	–	20.81	–	0.04	–	–	99.69
KC14-483/3	34.47	–	–	44.88	190	20.49	–	–	–	–	99.91
KC14-44-483/3	34.63	–	–	44.28	–	20.53	–	0.06	–	–	99.55
KC14-483/5	34.08	–	–	45.74	3100	19.77	–	–	–	–	99.96
KC14-483/5	34.10	0.04	–	45.49	1690	20.39	–	0.41	–	–	100.59
KC14-483/5	34.41	–	–	44.37	2310	20.95	–	0.12	–	–	100.11
KC14-483/5	33.75	–	–	45.86	2190	20.13	–	–	–	–	99.98
KC14-483/5	34.12	–	–	45.70	2090	20.41	–	–	–	–	100.51
KC14-483/5	34.01	–	–	45.82	1980	20.15	–	0.04	–	–	100.23
KC14-489/2	33.78	–	–	44.62	–	20.82	–	–	–	–	99.24
KC14-489/2	33.91	–	–	44.57	–	20.99	–	–	–	–	99.55
KC14-489/2	33.66	–	–	44.78	–	20.78	–	–	–	–	99.26
KC14-489/5	34.27	–	–	44.46	580	21.18	–	0.04	–	–	100.01
KC14-489/5	34.34	–	–	45.09	360	20.98	–	–	–	–	100.46
KC14-489/5	34.54	–	–	44.75	380	21.36	–	–	–	–	100.72
KC14-489/5	34.79	–	–	44.19	230	21.20	–	–	–	–	100.27
KC14-497/1	34.56	–	–	44.43	400	21.22	–	0.28	–	–	100.55
KC14-497/1	34.04	–	–	45.17	1140	20.70	–	0.09	–	–	100.15
KC14-497/1	34.33	–	–	44.98	260	20.82	–	0.08	–	–	100.28
KC14-497/2	34.69	–	–	44.12	–	21.14	–	0.04	–	–	100.02
KC14-497/2	34.10	–	–	43.38	–	21.65	–	0.32	–	–	99.52
KC14-497/2	33.91	–	–	44.81	–	20.97	–	–	0.11	–	99.82
KC14-497/2	33.89	–	–	43.20	–	21.67	–	0.45	–	–	99.26

Table 2
Electron probe microanalysis results (Au — ppm; other element — wt.%) for pyrite from the Hat Han deposit.

Samp. no	Fe	Co	Ni	As	Au	S	Ag	Sb	Zn	Cu	Total
Detection limit	0.025	0.030	0.036	0.050	400	0.012	0.045	0.037	0.047	0.040	
KC14-481	46.27	–	–	–	–	52.94	–	–	–	–	99.22
KC14-481	46.16	0.09	–	0.44	–	52.55	–	–	–	–	99.26
KC14-484	46.73	–	–	–	–	53.82	–	0.05	–	–	100.61
KC14-484	46.58	–	–	–	–	53.20	–	–	–	–	99.80
KC14-484	46.01	–	–	–	–	53.58	–	–	–	–	99.66
KC14-484	46.26	–	–	–	–	53.06	–	–	–	–	99.35
KC14-484	46.24	–	–	–	–	53.10	–	0.12	–	–	99.53
KC14-496	45.94	–	–	0.65	–	51.97	–	–	–	–	98.60
KC14-496	45.94	–	–	0.71	–	52.21	–	–	–	–	98.87
KC14-496	45.53	–	–	1.15	–	51.90	–	–	–	–	98.59
KC14-496	46.07	–	–	0.27	–	52.65	–	–	–	–	99.01
KC14-478/2	46.05	–	–	–	–	53.11	–	–	–	–	99.19
KC14-478/2	45.51	–	–	1.35	–	52.09	–	0.06	–	–	99.05
KC14-478/2	46.32	–	–	–	–	53.56	–	–	–	–	99.90
KC14-478/3	46.50	–	–	–	–	53.22	–	–	–	–	99.73
KC14-478/3	46.21	–	–	–	–	53.55	–	0.07	–	–	99.84
KC14-478/3	46.31	–	–	–	–	53.67	–	–	–	–	99.99
KC14-480/2	46.77	–	–	–	–	53.25	–	0.06	–	–	100.09
KC14-480/2	46.59	–	–	–	–	53.40	–	–	–	–	100.05
KC14-480/2	46.71	–	–	–	–	53.35	–	0.04	–	–	100.11
KC14-480/3	46.06	–	–	0.55	350	51.49	–	–	–	–	98.14
KC14-480/3	46.18	–	–	1.12	120	51.21	–	–	–	–	98.57
KC14-480/3	46.00	0.11	–	1.15	140	51.31	–	–	–	–	98.63
KC14-480/3	46.09	–	–	1.26	–	51.46	–	–	–	–	98.85
KC14-480/3	46.06	–	–	1.35	490	51.25	–	–	–	–	98.75
KC14-483/3	46.32	–	–	–	320	53.08	–	–	–	–	99.46
KC14-483/3	46.40	–	–	1.14	–	51.77	–	–	–	–	99.33
KC14-483/3	46.83	–	–	–	120	52.27	–	–	–	–	99.11
KC14-483/3	46.05	–	–	1.41	–	52.37	–	–	–	–	99.86
KC14-483/5	46.46	–	–	–	1360	52.36	–	–	–	–	99.00
KC14-483/5	46.55	–	–	0.82	1640	51.69	–	–	–	–	99.27
KC14-483/5	46.36	–	–	0.78	1690	51.80	–	–	–	–	99.13
KC14-483/5	46.38	–	–	0.84	1680	51.88	–	–	–	–	99.30
KC14-483/5	46.58	–	–	0.56	1440	52.00	–	–	–	–	99.33
KC14-489/2	46.34	–	–	0.33	–	52.49	–	–	–	–	99.19
KC14-489/2	46.64	–	–	0.46	–	52.02	–	–	–	–	99.15
KC14-489/2	46.34	–	–	–	–	53.18	–	0.10	–	–	99.67
KC14-489/4	45.99	–	–	0.97	–	51.88	–	0.01	0.32	–	99.17
KC14-489/4	46.38	–	–	1.19	–	51.74	–	–	0.14	–	99.49
KC14-489/4	46.45	–	–	0.87	–	51.83	–	–	–	–	99.17
KC14-489/4	46.42	–	–	0.91	–	51.94	–	–	–	–	99.35
KC14-489/5	46.46	–	–	0.90	–	51.78	–	–	–	–	99.19
KC14-489/5	46.18	–	–	1.02	140	52.67	–	–	0.05	–	99.96
KC14-489/5	46.64	–	–	–	–	53.34	–	–	–	–	100.04
KC14-497/1	46.58	–	–	–	–	53.54	–	–	–	–	100.15
KC14-497/1	46.21	–	–	–	–	53.54	–	0.09	–	–	99.85
KC14-497/1	46.46	–	–	–	–	53.23	–	0.05	–	–	99.77
KC14-497/2	45.86	–	–	0.72	–	52.87	–	–	–	–	99.49
KC14-497/2	46.37	–	–	0.77	–	52.17	–	–	–	–	99.38
KC14-497/2	46.57	–	–	0.50	–	52.48	–	–	–	–	99.57
KC14-497/2	46.75	–	–	–	–	53.11	–	–	–	–	99.90
KC14-497/3	46.51	–	–	–	–	53.06	–	–	–	–	99.58
KC14-497/3	46.82	–	–	–	–	53.27	–	–	–	–	100.15
KC14-497/3	46.29	–	–	–	–	53.14	–	–	–	–	99.48

The main gold-bearing iron sulphide in Carlin-like deposits in southern China is arsenic pyrite, followed by arsenopyrite (Peters et al., 2007). Throughout studies of the Hat Han gold deposit, regardless of using highly sensitive instruments such as optical and SEM, native gold had never been found. However, EPMA analysis conducted on arsenopyrite and pyrite revealed Au concentrations at 3100 and 1700 ppm, respectively.

Arsenopyrite bearing high concentration of gold was reported for large-scale gold deposits localised in strongly deformed black shale formations with various ages (Ashley et al., 2000; Genkin et al., 1998; Volkov et al., 2006). In some deposits, the position of gold in the arsenopyrite structural network was identified; in others, not only the structural position but also the position of gold metal particles in the arsenopyrite structural network was also defined (Boiron et al., 1989; Cabri et al., 1989; Genkin et al., 1998; Maddox et al., 1998; Murzin

et al., 2003; Reich et al., 2005; Volkov et al., 2006; Yang et al., 1998). Indirect proof of the chemical binding of gold is its connection with the major components of arsenopyrite. At some deposits the Au–As connection is well-established (Cabri et al., 1989; Fleet and Mumin, 1997; Maddox et al., 1998), but at others the relationship is unidentified (Ashley et al., 2000). Some authors report that gold-bearing arsenopyrite is typically poor in iron (Fleet and Mumin, 1997).

At the Hat Han deposit arsenopyrite contains less As than it theoretically should. However, this feature of gold-bearing arsenopyrite is widely observed at many orogenic gold deposits (Genkin et al., 1998; Tyukova and Voroshin, 2007). Fe concentrations may vary slightly, but generally correspond to theoretical compositions.

Analysis of the relationship of gold content in arsenopyrite to the concentration of the main components (F, As, S) shows a positive correlation between Au and As (and negative correlation between Au and

Table 3
Major-element and trace-element data from the analysed host unaltered gabbro and different types of ore.

Analyte symbol	Unit symbol	Detection limit	Host gabbro	Gold ore						Complex ore				Antimony ore	
			KC14-479/1	KC14-478/3	KC14-479/4	KC14-483/3	KC14-496	KC14-480/2	KC14-481	KC14-480/3	KC14-483/5	KC14-479/2	KC14-478/2	KC14-483/4	KC14-488
Au	ppb	1	1	8190	2870	3920	6040	9720	8140	6760	12100	1460	19800	26	124
Ag	ppm	0.05	0.39	0.71	0.83	0.44	2.99	0.54	0.51	0.65	0.67	1.07	0.95	0.27	18.4
Cu	ppm	0.2	24.8	12.6	14.9	8	18.9	15.4	11.2	9.8	12.6	8.4	48.5	12.6	152
Cd	ppm	0.1	0.2	0.1	0.1	0.2	2.9	0.1	0.1	0.2	4.8	0.2	0.5	0.8	16.9
Pb	ppm	0.5	16	14.2	11.4	3.5	114	6.7	18.6	7.4	28.8	0.5	45.4	42.7	1410
Ni	ppm	0.5	14.7	6.2	9.8	13.8	13.9	8.2	3.8	6.3	5.8	1.3	6.5	15.2	3.8
Zn	ppm	0.5	112	58.7	43.7	33.8	340	34.4	30.8	71.4	1520	9.1	168	405	3340
S	%	0.01	0.16	5.45	3.26	3.55	5.27	6.03	1.54	2.65	5.25	6.06	7.39	0.87	2.26
Al	%	0.01	7.34	3.14	4.52	7.9	6.61	4.97	3.72	6.73	4.68	0.64	4.08	6.89	0.37
As	ppm	0.5	49.4	23900	10100	12700	25000	27400	24900	11600	18300	5050	46300	162	1030
Sb	ppm	0.1	26	732	776	77.7	223	366	158	2240	4960	>10000	>10000	>10000	>10000
Ba	ppm	1	305	94	137	142	98	103	130	175	100	1	90	185	7
Be	ppm	0.1	1.6	2.3	2.5	3	3.1	2.7	1.7	3.6	1.8	0.7	2.1	2.6	0.4
Br	ppm	0.5	0.5	0.5	0.5	0.5	0.5	0.5	0.5	0.5	0.5	0.5	0.5	0.5	0.5
Ca	%	0.01	4.94	1.18	3.32	0.98	1.01	2.03	0.13	5.93	0.02	0.2	1.35	1.73	0.01
Co	ppm	0.1	42.7	21.8	24.2	18.3	17.4	42.4	9.9	35.9	3.8	0.3	41.5	11.8	0.2
Cr	ppm	1	1	8	1	1	1	8	1	10	1	1	4	1	6
Cs	ppm	0.05	3.44	2.42	4.32	2.78	2.77	2.64	1.46	3.04	0.92	0.6	2.2	2.81	0.08
Fe	%	0.01	9.04	8.01	6.85	5.02	7.58	9.74	6.64	8.93	6.16	0.01	10	2.3	0.01
Hf	ppm	0.1	1	0.7	1.4	4.5	1.7	1	0.4	3.1	2	0.1	0.6	2.6	0.1
K	%	0.01	1.33	1.57	1.94	4	3.31	2.36	1.71	3.38	2.1	0.12	1.84	3.16	0.03
Mg	%	0.01	2.38	0.33	1.06	0.48	0.42	0.6	0.14	1.57	0.12	0.05	0.4	0.57	0.01
Mn	ppm	1	1270	259	670	249	224	415	279	1170	66	51	246	570	75
Na	%	0.01	1.41	0.04	0.07	0.04	0.03	0.02	0.01	0.02	0.05	0.51	0.13	0.04	0.52
P	%	0.001	0.072	0.032	0.034	0.044	0.07	0.038	0.034	0.066	0.011	0.001	0.018	0.054	0.001
Rb	ppm	0.2	87.9	96.8	118	192	144	111	95.5	118	104	8.2	98.3	137	2.5
Sc	ppm	0.1	38.1	17.4	20.7	16.1	14.6	25.7	15.5	36.2	7.7	0.1	18	19.1	0.1
Se	ppm	0.1	0.7	1.3	1.3	1.3	1.7	1.2	0.3	0.7	0.9	1.3	1.5	0.4	1.3
Ta	ppm	0.1	0.1	0.1	0.1	0.1	0.1	0.1	0.1	0.3	0.1	0.1	0.1	0.1	0.1
Ti	%	0.01	0.18	0.98	0.66	0.66	0.43	0.62	0.48	0.74	0.13	0.01	0.39	0.25	0.01
Th	ppm	0.1	9.6	5.3	0.1	15.6	14.1	6.6	2.8	13.5	21.3	0.2	5.4	27.5	0.5
V	ppm	2	116	311	205	150	112	383	196	184	34	2	273	39	2
U	ppm	0.1	1.4	0.8	0.9	3.8	3.8	1	0.6	1.4	3	0.1	0.9	3.1	0.1
W	ppm	1	1	147	50	1	1	143	1	221	1	1	1	1	1
Ga	ppm	0.1	17.5	10.4	11.5	20.7	18.5	13.7	9.3	20.6	11.3	0.9	11.2	16.6	0.4
Ge	ppm	0.1	0.2	0.3	0.6	0.3	0.3	0.2	0.2	0.9	0.4	0.4	0.3	0.4	0.8
Hg	ppb	10	1290	4070	1770	3420	3400	2590	2450	3120	4290	2340	3390	1060	4630
Li	ppm	0.5	24	9.5	8.5	3.5	4.8	6.3	3.9	3.2	1.4	0.5	4.9	2.8	0.5
Sr	ppm	0.2	126	51.5	133	43.7	48.6	72.8	19.2	233	12	7	53	98	2.8
Tl	ppm	0.05	0.41	1.48	1.53	1.28	1.57	1.74	0.48	0.89	0.7	0.75	1.34	0.85	0.2
Y	ppm	0.1	34.5	19	15.7	33.1	36	21.2	8.9	16.2	28.7	2.8	19.6	34.5	1
Zr	ppm	1	38	71	78	225	160	85	72	146	127	1	74	104	2
La	ppm	0.1	16	9.2	11.2	29	26.2	10.6	6.5	10.8	16.2	0.1	10	25	0.1
Ce	ppm	0.1	33.3	19.2	23	59.3	52.9	22.3	12.8	25.3	34	1.2	22.1	52.1	1.1
Pr	ppm	0.1	4.2	2.4	2.9	7.3	6.4	2.8	1.5	3.4	4.1	0.2	2.8	6.5	0.2
Nd	ppm	0.1	16.9	9.5	11.3	27	23.9	11.2	5.7	13.7	14.6	0.6	11	24.9	0.6
Sm	ppm	0.1	4.2	2.2	2.4	5.7	5.2	2.7	1.3	3.3	3.2	0.1	2.4	5.6	0.2
Eu	ppm	0.05	1.3	0.71	0.67	1	1.11	0.81	0.32	0.9	0.57	0.06	0.76	1.07	0.05
Gd	ppm	0.1	5.7	2.7	2.6	5.5	5.8	3.4	1.4	3.5	4	0.2	3.1	5.9	0.1
Dy	ppm	0.1	6.5	3.4	2.8	5.7	6.5	3.9	1.7	3.2	4.8	0.4	3.6	6	0.2
Tb	ppm	0.1	1	0.5	0.4	0.9	0.9	0.6	0.2	0.5	0.7	0.1	0.5	0.9	0.1
Ho	ppm	0.1	1.4	0.8	0.6	1.2	1.4	0.9	0.4	0.7	1	0.1	0.8	1.3	0.1
Er	ppm	0.1	4.2	2.3	1.9	3.7	4.2	2.6	1.1	2	2.8	0.3	2.4	3.7	0.1
Tm	ppm	0.1	0.6	0.3	0.3	0.6	0.6	0.4	0.2	0.3	0.4	0.1	0.4	0.6	0.1
Yb	ppm	0.1	3.4	1.8	1.6	3.3	3.5	2.2	1	1.8	2.2	0.3	1.9	3	0.1
Lu	ppm	0.1	0.6	0.3	0.3	0.5	0.6	0.4	0.2	0.3	0.3	0.1	0.3	0.5	0.1

Table 4

Sulphur isotope compositions of arsenopyrites, pyrites and stibnite from the Hat Han deposit.

Samp. no	Mineral	d34SV-CDT‰
KC14-483/3	Arsenopyrite	7.3
KC14-478/3	Arsenopyrite	9.2
KC14-480/2	Arsenopyrite	6.4
KC14-489/7	Arsenopyrite	6.1
KC14-478/2	Arsenopyrite	6.5
KC14-483/2	Pyrite	6.8
KC14-489/5	Pyrite	7.9
KC14-483/3	Pyrite	7.0
KC14-478/2	Pyrite	5.5
KC14-768	Diagenetic pyrite	7.3
KC14-489/4	Stibnite	5.1
KC14-497/2	Stibnite	3.3
KC14-478/1	Stibnite	6.6
KC14-488	Stibnite	3.3
KC14-479/2	Stibnite	0.3

Note: (1) All values are reported as standard d34S notation relative to Canyon Diablo Troilite (V-CDT); and (2) analytical uncertainty is within ± 0.2‰.

S) (Fig. 6). The Au concentration in arsenopyrite does not depend on Fe content. This relationship suggests that Au is present in arsenopyrite in the chemically bound form. Yang et al. (1998) postulate that chemically bound gold occurs as octahedra, most likely of $AuAs_2$, likely of AuAsS, and less likely of AuS_2 in arsenopyrite or in pyrite.

In general, the gold concentration in arsenopyrite at the Hat Han deposit was determined according to the following factors: (i) the shortage of As in the observed chemical composition of arsenopyrite compared to the theoretical composition leads to defects in the crystal structure of arsenopyrite (Tyukova and Voroshin, 2007); and (ii) the participation of Au in the form of $AuAs_2$ in arsenopyrite (Yang et al., 1998) establishes the positive correlation between Au and As.

The average concentration of gold in arsenopyrite is closely related to gold concentration in the ore (Fig. 13). This suggests that gold-bearing sulphides have a major role in gold concentration at the Hat Han deposit.

Compared with arsenopyrite, pyrite at the Hat Han deposit contains slightly less gold. The maximum Au concentration in pyrite is ~1700 ppm. Using data from Reich et al. (2005) it may be assumed that much of the gold in pyrite is chemically bound while a minor portion occurs as nanoparticles of native Au (Au^0) (Fig. 14). This is indicated by the fact that high gold concentration in pyrite does not depend on the concentrations of major elements (Fe, S), and Sb and As (Fig. 7). However, as mentioned above, there may be a positive correlation between Au and As in pyrite observed for low-concentration data (near or under the detection limit for Au).

As shown in Figs. 6 and 7 shows the data, including below the detection limit of EPMA, as an alternative illustration, additional logarithmic graphs show the dependence between Au vs. As, and Au vs. S for pyrite and arsenopyrite. To construct these graphs, only reliable data acquired above the EPMA detection limit are used. Fig. 15 shows the discrete between Au vs. S and Au vs. As in pyrite. Whereas, for arsenopyrite there is a weak positive correlation between gold and arsenic and a negative correlation between Au and S.

In summary, although lacking in visible native gold, gold-bearing sulphide (arsenopyrite and pyrite) have a major role in gold concentration at the Hat Han deposit. Gold in arsenopyrite may exist as chemically bound forms, such as octahedral $AuAs_2$; whereas in pyrite, aside from being chemically bound, gold may occasionally be present as nanoparticles of native Au (Au^0). The genetic relation between gold and arsenopyrite and arsenic pyrite was clearly confirmed by correlation of Au and As in the ore.

5.5. Genetic model

Our research shows that the Hat Han deposit is an archetypal sediment-hosted gold deposit. Its characteristic features include: (i) the main minerals are arsenopyrite and pyrite; (ii) major gold-bearing sulphides are the sole gold-bearing components; (iii) antimony mineralisation overlapped early gold ore mineralisation; (iv) ore formation processes were related to metasomatic activities; and (v) sulphidation of Fe-bearing minerals in the host rocks was the major sulphide formation mechanism.

On the other hand, the deposit is hosted in a mafic magmatic rock, which suggests that the deposit may have a genetic relation to the igneous rock and therefore may have a different genesis to other deposits in the Song Hien sedimentary basin as well as the Nanpanjang basin in China. There are a number of examples of deposits associated with igneous rocks such as, the Twin Creek (Bloomstein et al., 1991; Thoreson et al., 2000), Betze (Leonardson and Rahn, 1996; Peters et al., 1998), and the Jimba, Badu and Anna deposits in the "golden triangle", southwestern China (Dong et al., 2014; Li et al., 2014; Peters, 2002; Peters et al., 2007). To date, many of the explanations proposed for this formation model are ambiguous. This study shows that the possible source of sulphur and ore components is sedimentary, not igneous. This explanation may imply that the Hat Han deposit in the Song Hien rift basin may have a structural relationship to the Nanpanjang basin in southwestern China. The analogy of mineralogical and geochemical characteristics in the Hat Han deposit to those in the Nanpanjang deposits suggests that the genesis of the Hat Han gold deposit is not related to the Cao Bang mafic magmatism; instead, the latter serves only as the ore host rock. The geochemical results presented above indicate that only the gabbro host rock supplies the iron required for sulphide formation. With regard to ore genesis, the Hat Han gold deposit in the Song Hien rift basin was generated in a similar way to Carlin-style sediment-hosted gold deposits. However, there are many similar typomorphic features between the Hat Han deposit and Carlin-like deposits in the Nanpanjang sedimentary basin in China.

6. Conclusions

The Hat Han ore deposits were formed following the introduction of gold, arsenic, and sulphur by hydrothermal fluids; whereas the sulphide was formed by iron taken from the gabbro host rock.

Sulphur isotopic compositions in sulphide are similar to those in carbonaceous shale, suggesting that the sulphur was 'borrowed' from sedimentary rocks in filling the rift basin.

Gold-bearing sulphides (pyrite and arsenopyrite) are the main form of Au presence in the ore.

Gold in pyrite is present as Au^{+1}, and a minor amount as nanoparticles of native Au (Au^0); whereas in arsenopyrite, gold is chemically bound as the octahedral complex $AuAs_2$.

The Hat Han deposit can be categorised as an orogenic gold deposit that might be produced by Carlin-style gold mineralisation, analogous to those in southern China (e.g. Chen et al., 2015b; Dong et al., 2014; Gu et al., 2012; Li et al., 2014; Su et al., 2009); therefore, its formation may be related to the Indosinian Orogeny.

References

Ashley, P.M., Creagh, C.J., Ryan, C.G., 2000. Invisible gold in ore and mineral concentrates from the Hillgrove gold–antimony deposits, NSW Australia. Mineral. Deposita 35 (4), 285–301.

Bloomstein, E.I., Massingill, G.L., Parrat, R.L., Peltonen, D.R., 1991. Discovery, geology, and mineralization of the Rabbit Creek gold deposit, Humboldt County, Nevada. In: Raines, G.L., Lisle, R.W., Schafer, R.W., Wilkinson, W.H. (Eds.), Geology and Ore Deposits of the Great Basin, Symposium Proceedings Vol. 2. Geological Society of Nevada, Reno, pp. 821–843.

Boiron, M.C., Cathelineau, M., Trescases, J.J., 1989. Conditions of gold bearing arsenopyrite crystallization in Villeranges basin, Marche-Combrailles shear zone, France: a mineralogical and fluid inclusion study. Econ. Geol. 84 (5), 1340–1362.

Cabri, L.J., Chryssoulis, S.L., De Villiers, J.P.R., LaFlamme, J.H.G., Buseck, P.R., 1989. The nature of «invisible» gold in arsenopyrite. Can. Mineral. 27 (3), 353–362.

Chang, Z., Large, R.R., Maslennikov, V., 2008. Sulfur isotopes in sediment-hosted orogenic gold deposits: evidence for an early timing and a seawater sulfur source. Geology 36, 971–974.

Chen, M., Mao, J., Li, C., Zhang, Z., Dang, Y., 2015b. Re–Os isochron ages for arsenopyrite from Carlin-like gold deposits in the Yunnan–Guizhou–Guangxi "golden triangle", southwestern China. Ore Geol. Rev. 64, 316–327.

Chen, M., Zhang, Z., Santosh, M., Dang, Y., Zhang, W., 2015a. The Carlin-type gold deposits of the "golden triangle" of SW China: Pb and S isotopic constraints for the ore genesis. J. Asian Earth Sci. 103, 115–128.

Chen, M.H., Mao, J.W., Bierlein, F.P., Norman, T., Uttley, P.J., 2011. Structural features and metallogenesis of the Carlin-type Lannigou gold deposit, Guizhou Province, China. Ore Geol. Rev. 43 (1), 217–234.

Dong, W.D., Su, W.C., Shen, N.P., Cai, J.L., 2014. Geological characteristics and fluid inclusions of Anna gold deposit in Funing, Yunnan. ACROFI 2014, Xi'an, China.

Dovzhikov, A.E., My, B.P., Vasilevskaya, E.D., Zhamoida, A.I., Ivanov, G.V., Izokh, E.P., Huu, L.D., Mareichev, A.M., Chien, N.V., Tri, N.T., Luong, T.D., Quang, P.V., Long, P.D., 1965. Geology of Northern Vietnam (in Russian) Pub. House Science & Techn., Hanoi.

Faure, M., Lepvrier, C., Nguyen, V.V., Vu, T.V., Lin, W., Chen, Z., 2014. The South China block–Indochina collision: where, when, and how? J. Asian Earth Sci. 79, 260–274.

Fleet, M.E., Mumin, A.H., 1997. Gold-bearing arsenian pyrite and marcasite and arsenopyrite from Carlin Trend gold deposits and laboratory synthesis. Am. Mineral. 82 (1–2), 182–193.

Galfetti, T., Bucher, H., Martini, R., Hochuli, P., Weissert, H., Crasquin-Soleau, S., Brayard, A., Goudemand, N., Brühwiler, T., Guodun, K., 2008. Evolution of Early Triassic outer platform paleoenvironments in the Nanpanjiang basin (South China) and their significance for the biotic recovery. Sediment. Geol. 204, 36–60.

Genkin, A.D., Bortnikov, N.S., Cabri, L.J., Wagner, F.E., Stanley, C.J., Safonov, Y.G., McMahon, G., Freidl, J., Kerzin, A.I., Gamyanin, G.N., 1998. A multidisciplinary study of invisible gold in arsenopyrite from four mesothermal gold deposits in Siberia, Russian Federation. Econ. Geol. 93, 463–487.

Grant, J.A., 1986. The isocon diagrams—a simple solution to Gresen's equation for metasomatic alteration. Econ. Geol. 42, 91–106.

Gresens, R.L., 1967. Composition–volume relationships of metasomatism. Chem. Geol. 2, 47–55.

Gu, X.X., Zhang, Y.M., Li, B.H., Dong, S.Y., Xue, C.J., Fu, S.H., 2012. Hydrocarbon- and ore-bearing basinal fluids: a possible link between gold mineralization and hydrocarbon accumulation in the Youjiang basin, South China. Mineral. Deposita 47, 663–682.

Guangxi BGMR (Bureau of Geology and Mineral Resources), 1985. Regional geology of Guangxi Zhuang Autonomous Region. Geological Memoirs, Series Vol. 1, p. 3 (853 pp.).

Hoa, T.T., 2007. Within-Plate Magmatism of Northern Vietnam and Its Metallogeny (Dissertation) VS Sobolev Institute of Geology and Mineralogy SB RAS, Novosibirsk (in Russian).

Hoa, T.T., Izokh, A.E., Polyakov, G.V., Borisenko, A.S., Anh, T.T., Balykin, P.A., Phuong, N.T., Rudnev, S.N., Van, V.V., Nien, B.A., 2008. Permo-Triassic magmatism and metallogeny of Northern Vietnam in relation to the Emeishan plume. Russ. Geol. Geophys. 49, 480–491.

Hofstra, A.H., Cline, J.S., 2000. Characteristics and models for Carlin-type gold deposits. In: Hagemann, S.G., Brown, P.E. (Eds.), Rev. in Econ. Geol. vol. 13, pp. 163–214

Hofstra, A.H., Leventhal, J.S., Northrop, H.R., Landis, G.P., Rye, R.O., Birak, D.J., Dahl, A.R., 1991. Genesis of sediment-hosted disseminated gold deposits by fluid mixing and sulfidization: chemical-reaction path modeling of ore-depositional processes documented in the Jerritt Canyon district. Nev. Geol. 19, 36–40.

Holse, W.T., Magaritz, M., Ripperdan, R.L., 1996. Global isotopic events. In: Walliser, O.H. (Ed.), Global Events and Event Stratigraphy in the Phanerozoic. Springer-Verlag, Berlin, pp. 1–201.

Izokh, A.E., Polyakov, G.V., Hoa, T.T., Balykin, P.A., Phuong, N.T., 2005. Permian–Triassic ultramafic–mafic magmatism of Northern Vietnam and Southern China as expression of plume magmatism. Russ. Geol. Geophys. 46, 942–951 (in Russian).

Large, R.R., Bull, S.W., Maslennikov, V.V., 2011. A carbonaceous sedimentary source-rock model for Carlin-type and orogenic gold deposits. Econ. Geol. 106 (3), 331–358.

Large, R.R., Maslennikov, V.V., Robert, F., Danyushevsky, L.V., Scott, R.J., Chang, Z., 2007. Multi-stage sedimentary and metamorphic origin of pyrite and gold in the giant Sukhoi Log deposit, Lena Goldfield, Russia. Econ. Geol. 102, 1233–1267.

Leloup, P.H., Lacassin, R., Tapponnier, P., Schärer, U., Zhong, D., Liu, X., Zhang, L., Ji, S., Trinh, P., 1995. The Ailaoshan-Red River shear zone (Yunnan, China), Tertiary transform boundary of Indochina. Tectonophysics 252, 3–84.

Leonardson, R.W., Rahn, J.E., 1996. Geology of the Betze-Post gold deposits, Eureka County, Nevada. In: Coyner, A.R., Fahey (Eds.), Geology and Ore Deposits of the American Cordillera: Geological Society of Nevada, Symposium Proceedings, Reno/Sparks, Nevada, pp. 61–94.

Lepvrier, C., Faure, M., Voung, N.V., Tich, V.V., Lin, W., Thang, T.T., Phuong, T.H., 2011. North-directed Triassic nappes in Northeastern Vietnam (East Bac Bo). J. Asian Earth Sci. 41, 56–68.

Lepvrier, C., Maluski, H., Voung, N.V., Roques, D., Axente, V., Rangin, C., 1997. Indosinian NW-trending shear zones within the Truong Son belt (Vietnam): [40]Ar–[39]Ar Triassic ages and Cretaceous to Cenozoic overprints. Tectonophysics 283, 105–127.

Lepvrier, C., Vuong, N.V., Maluski, H., Thi, P.T., Tich, V.V., 2008. Indosinian tectonics in Vietnam. Compt. Rendus Geosci. 340, 94–111.

Li, P., Pang, B., Wang, B., Li, Y., Zhou, Y., Lv, J., Ma, J., 2014. Fluid inclusions and rare earth elements of the Badu gold deposit, Guangxi, China: implications for mineralization. Acta Geol. Sin. (Engl. Ed.) 88 (Suppl. 2), 1118–1119.

Liu, J., Tran, M., Tang, Y., Nguyen, Q.L., Tran, T.H., Wu, W., Chen, J., Zhang, Z., Zhao, Z., 2012. Permo-Triassic granitoids in the northern part of the Truong Son belt, NW Vietnam: geochronology, geochemistry and tectonic implications. Gondwana Res. 122, 628–644.

Maddox, L.M., Bancroft, G.M., Scaini, M.J., Lorimer, J.W., 1998. Invisible gold: comparison of Au deposition on pyrite and arsenopyrite. Am. Mineral. 83 (11–12), 1240–1245.

Murzin, V.V., Semenkin, V.A., Pikulev, A.I., Mil'der, O.B., Sustavov, S.G., Krinov, D.I., 2003. Mössbauer spectroscopic evidence for nonequivalent sites of iron atoms in gold-bearing arsenopyrite. Geochem. Int. 41 (8), 812–820.

Novozhilov, Yu.I., Gavrilov, A.M., 1999. Gold–Sulfide Deposits in Carbonaceous Terrigenous Strata. TsNIGRI, Moscow (in Russian).

Peng, Y., Gu, X., Zhang, Y., Liu, L., Wu, C., Chen, S., 2014. Ore-forming process of the Huijiabao gold district, southwestern Guizhou Province, China: evidence from fluid inclusions and stable isotopes. J. Asia Earth Sci. 93, 89–101.

Peters, S.G., 2002. Geology, geochemistry, and geophysics of sedimentary-hosted Au deposits in P.R. China. U.S. Geological Survey Open-File Report, 02-131 http://geopubs.wr.usgs.gov/open-file/of02-131/.

Peters, S.G., Ferdock, G.C., Woitsekhowskaya, M.B., Leonardson, R., Rahn, J., 1998. Oreshoot zoning in the Carlin-type Betze orebody, Goldstrike Mine, Eureka County, Nevada. U.S. Geological Survey Open-File Report 98-620, p. 49.

Peters, S.G., Huang, J.Z., Li, Z.P., Jing, C.G., 2007. Sedimentary rock-hosted Au deposits of the Dian–Qian–Gui area, Guizhou, and Yunnan Provinces, and Guangxi District, China. Ore Geol. Rev. 31, 170–204.

Polyakov, G.V., Shelepaev, R.A., Hoa, T.T., Izokh, A.E., Balykin, P.A., Phuong, N.T., Hung, T.Q., Nien, B.A., 2009. The Nui Chua layered peridotite gabbro complex as manifestation of Permo-Triassic mantle plume in northern Vietnam. Russ. Geol. Geophys. 50, 501–516.

Reich, M., Kesler, S.E., Utsunomiya, S., Palenik, C.S., Chryssoulis, S.L., Ewing, R.C., 2005. Solubility of gold in arsenian pyrite. Geochim. Cosmochim. Acta 69 (11), 2781–2796.

Saunders, J.A., Hofstra, A.H., Goldfarb, R.J., Reed, M.H., 2014. Geochemistry of hydrothermal gold deposits. In: Holland, H.D., Turekian, K.K. (Eds.), second ed. Treatise on Geochemistry vol. 13. Elsevier, Oxford, pp. 383–424.

Simon, G., Kesler, S.E., Chryssoulis, S., 1999. Geochemistry and textures of gold-bearing arsenian pyrite, Twin Creeks, Nevada: implications for deposition of gold in Carlin-type deposits. Econ. Geol. 94, 405–422.

Su, W., Xia, B., Zhang, H., Zhang, X., Hu, R., 2008. Visible gold in arsenian pyrite at the Shuiyindong Carlin-type gold deposit, Guizhou, China: implications for the environment and processes of ore formation. Ore Geol. Rev. 33, 667–679.

Su, W.C., Heinrich, C.A., Pettke, T., Zhang, X.C., Hu, R.Z., Xia, B., 2009. Sediment-hosted gold deposits in Guizhou, China: products of wall-rock sulfidation by deep crustal fluids. Econ. Geol. 104, 73–93.

Tapponnier, P., Lacassin, R., Leloup, H., Schärer, U., Zhong, D., Liu, X., Ji, S., Zhang, L., Zhong, J., 1990. The Ailaoshan-Red river metamorphic belt: tertiary left-lateral shear between Indochina and South China. Nature 343, 431–437.

Thoreson, R.F., Jones, M.E., Breit, F.J., Doyle-Kunkel, M.A., Clarke, L.J., 2000. The geology and gold mineralization of the Twin Creeks gold deposits, Humboldt County, Nevada. In: Crafford, A.E.J. (Ed.), Geology and Ore Deposits of the Getchell Region Humboldt County, Nevada: Geological Society of Nevada Symposium Field Trip Guidebook. Vol. 9, pp. 85–111.

Geology and earth resources of Vietnam. In: Tri, T.V., Vu, K. (Eds.), General Dept. of Geology, and Minerals of Vietnam. Publishing House for Science and Technology, Hanoi.

Tyukova, Ye.E., Voroshin, S.V., 2007. Arsenopyrite mineral composition and parageneses in ore deposit and host rocks throughout the Upper Kolyma River area (interpreting the genesis of sulfide mineral assemblages). Magadan, NEISRI FEB RAS (in Russian).

Vladimirov, A.G., Kruk, N.N., Smirnov, C.Z., Annikova, I.Y., Pavlova, G.G., Kuibida, M.L., Moroz, E.N., Sokolova, E.N., Anh, P.L., Astrelina, E.I., 2012. Petrology of the tin-bearing granite-leucogranites of the Piaoak massif, northern Vietnam. Petrology 20 (6), 545–566.

Volkov, A.V., Genkin, A.D., Goncharov, V.I., 2006. The forms of the presence of gold in the ores of the Natalka and May deposits (Northeast Russia). Russ. J. Pac. Geol. 25 (6), 18–29 (in Russian with English abstract).

Yang, S., Blum, N., Rahders, E., Zhang, Z., 1998. The nature of invisible gold in sulfides from the Xiangxa Au–Sb–W ore deposit in northwestern Hunan, People's Republic of China. Can. Mineral. 36, 1361–1372.

Zhang, R.Y., Lo, C.H., Chung, S.L., Grove, M., Omori, S., Iizuka, Y., Liou, J.G., Tri, T.V., 2013. Origin and tectonic implication of ophiolite and eclogite in the Song Ma Suture Zone between the South China and Indochina Blocks. J. Metamorph. Geol. 31, 49–62.

Zhang, X.C., Hofstra, A.H., Hu, R.-Z., Emsbo, P., Su, W., Ridley, W.I., 2005. Geochemistry and $\delta^{34}S$ of ores and ore stage iron sulfides in Carlin-type gold deposits, Dian-Qian-Gui area, China: implications for ore genesis. In: Mao, J.W., Bierlein, F.P. (Eds.), Mineral Deposits Research: Meeting the Global Challenge Vol. 2. Springer-Verlag, Heidelberg, pp. 1107–1110.

Zhong, H.R., Chao, S.W., Wu, B.X., Zhi, T.G., Hofstra, A.H., 2002. Geology and geochemistry of Carlin-type gold deposits in China. Mineral. Deposita 37, 378–392.

Zhou, T.H., Goldfarb, R.J., Phillips, G.N., 2002. Tectonics and metallogeny of gold deposits in China. Mineral. Deposita 37, 249–282.